SANDIA REPORT

SAND86—2808 • UC—23
Unlimited Release
Printed April 1988

Characterization of Two WESF Capsules After Five Years of Service

D. J. Sasmor, J. D. Pierce, G. L. Tingey,
H. E. Kjarmo, J. Tills, and D. C. McKeon

Prepared by
Sandia National Laboratories
Albuquerque, New Mexico 87185 and Livermore, California 94550
for the United States Department of Energy
under Contract DE-AC04-76DP00789

When printing a copy of any digitized SAND Report, you are required to update the markings to current standards.

SF2900Q(8-81)

Issued by Sandia National Laboratories, operated for the United States Department of Energy by Sandia Corporation.

NOTICE: This report was prepared as an account of work sponsored by an agency of the United States Government. Neither the United States Government nor any agency thereof, nor any of their employees, nor any of their contractors, subcontractors, or their employees, makes any warranty, express or implied, or assumes any legal liability or responsibility for the accuracy, completeness, or usefulness of any information, apparatus, product, or process disclosed, or represents that its use would not infringe privately owned rights. Reference herein to any specific commercial product, process, or service by trade name, trademark, manufacturer, or otherwise, does not necessarily constitute or imply its endorsement, recommendation, or favoring by the United States Government, any agency thereof or any of their contractors or subcontractors. The views and opinions expressed herein do not necessarily state or reflect those of the United States Government, any agency thereof or any of their contractors or subcontractors.

Printed in the United States of America
Available from
National Technical Information Service
U.S. Department of Commerce
5285 Port Royal Road
Springfield, VA 22161

NTIS price codes
Printed copy: A05
Microfiche copy: A01

Distribution
Category: UC-23

SAND86-2808
Unlimited Distribution
Printed April 1988

CHARACTERIZATION OF TWO WESF CAPSULES AFTER FIVE YEARS OF SERVICE

D. J. Sasmor
Radiation Physics and Diagnostics Division

J. D. Pierce
Transportation Systems Development and Testing Division
Sandia National Laboratories
Albuquerque, New Mexico 87185

G. L. Tingey and H. E. Kjarmo
Battelle Pacific Northwest Laboratories
Richland, Washington 99352

J. Tills
Jack Tills & Associates, Inc.
Albuquerque, New Mexico 87123

D. C. McKeon*
Sandia National Laboratories
Albuquerque, New Mexico 87185

Sandia National Laboratories
Albuquerque, NM 87115
Operated by
Sandia Corporation
for the
U.S. Department of Energy

*Present address: Schlumberger Well Services,
Houston, Texas 77252

ABSTRACT

Two Waste Encapsulation and Storage Facility (WESF) ^{137}Cs capsules have been analyzed destructively after five years of service in the Sandia Irradiator for Dried Sewage Solids (SIDSS). Analysis of these capsules was a joint undertaking of Sandia National Laboratories, Albuquerque (SNLA) and Battelle Pacific Northwest Laboratory (PNL) with assistance from Rockwell Hanford Operations (RHO). The program concentrated on studies of the inner capsule, inner capsule weld areas, and analysis of the CsCl salt.

No measurable corrosion was observed on the capsule wall or welds after the five years in the SIDSS Facility. The operating temperatures of the inner capsule wall were calculated to be between 140° and 180°C.

Radiochemistry and isotopic analyses provided data for specific activity calculations. There was good correlation between the measured calorimetry of the capsules before sectioning, 53 and 55 kCi, and the activity calculations, 54 and 59 kCi, respectively.

CONTENTS

Section		Page
1	INTRODUCTION	1
2	CAPSULE DATA AND HISTORY	2
3	CAPSULE DISASSEMBLY AND SAMPLE PROCUREMENT	5
4	SHIPPING CAPSULE CUTTING AND MATERIAL INVENTORY	11
5	MACRO EXAMINATION AND MECHANICAL THICKNESS MEASUREMENTS	12
6	METALLOGRAPHY SPECIMEN SECTIONING AND EXAMINATION	21
7	MICROPROBE ANALYSIS	35
8	ISOTOPIC AND CHEMICAL ANALYSIS OF THE SALT	36
9	CONCLUSION	41
10	REFERENCES	43
APPENDIX A	TEMPERATURE MODEL BASED ON SIDSS IRRAADIATOR CAPSULE CONFIGURATION	A-1
APPENDIX B	SPECIFICATION FOR SEAMLESS 316-L AUSTENITIC-STAINLESS STEEL TUBING FOR CESIUM CHLORIDE ENCAPSULATION	B-1

LIST OF FIGURES

Figure		Page
1	Detail of WESF Cesium-137 Source Capsule	3
2	Typical Cutting Schedule	6
3	Hot-End Weld and Inner Capsule	7
4	Depth of Salt from End Cap After First Cut	7
5	Surface of Salt and the Bottom of Shrinkage Hole at the One-Notch Location	8
6	Surface of Salt at the Two-Notch Location	8
7	Surface of Salt at the Three-Notch Location	9
8	Surface of Salt at the Four-Notch Location	9
9	Buoyant Mass During Dissolution	10
10	Detection Head and Anvil Plate	13
11	Capsule Wall Thickness Measurements for Capsule C-73	15
12	Capsule Wall Thickness Measurements for Capsule C-74	15
13	Capsule C-73, Ring 1	17
14	Capsule C-73, Ring 2	17
15	Capsule C-73, Ring 3	18
16	Capsule C-73, Ring 4	18
17	Capsule C-74, Ring 1	19
18	Capsule C-74, Ring 2	19
19	Capsule C-74, Ring 3	20
20	Capsule C-74, Ring 4	20
21	Metallographic Mounting Apparatus	21
22	Photomicrographs of Capsule C-73, Ring 2, As-Polished	22

LIST OF FIGURES (Continued)

Figure		Page
23	Photomicrographs of Capsule C-73, Ring 3, As-Polished	23
24	Photomicrographs of Capsule C-74, Ring 2, As-Polished	23
25	Photomicrographs of Capsule C-74, Ring 3, As-Polished	24
26	Photomicrograph of Capsule C-74 Top End-Cap Weld (In-Cell Weld)	24
27	Photomicrograph of Capsule C-74 Bottom End-Cap Weld (Out-of-Cell Weld)	25
28	Photomicrograph of Capsule C-73 Top End-Cap Weld (In-Cell Weld)	25
29	Photomicrographs of Capsule C-73, Ring 2, Etched	26
30	Photomicrographs of Capsule C-73, Ring 3, Etched	27
31	Photomicrographs of Capsule C-74, Ring 2, Etched	28
32	Photomicrographs of Capsule C-74, Ring 3, Etched	29
33	Photomicrographs of Zero-Time Capsule, Etched, 500X	30
34	Photomicrograph of Capsule C-73, Etched Section Center, 500X	31
35	Photomicrograph of Capsule C-74, Etched Section Center, 500X	31
36	Corrosion Rate of WESF Cesium Capsules	34
A.1	Gamma Source Plaque	A-2
A.2	WESF Capsule Geometries for R-θ Heat Transfer	A-2
A.3	Finite Element Mesh	A-3
A.4	Symmetry Configuration Temperature MAP (K) as a Function of θ & R	A-4
A.5	Asymmetric Configuration Temperature MAP (K) as a Function of θ & R	A-5

LIST OF FIGURES (Continued)

Figure		Page
A.6	Asymmetric Configuration Temperature MAP (K) as a Function of θ & R	A-6
A1.1	Decay Scheme for ^{137}Cs	A-12
A1.2	WESF Cesium Chloride Source Capsule	A-13

LIST OF TABLES

Table		Page
1	Historical Data for WESF Capsules	4
2	WESF Capsule Identification and Capsule Contents	11
3	Circumferential Thickness Measurements for Capsule C-73	14
4	Circumferential Thickness Measurements for Capsule C-74	14
5	Microdot Measurement of Metallographic Section	16
6	Standard and Measured Gauge Block Values	16
7	Estimates of Metal Attack	33
8	Metallography Section Thickness Measurements on Capsules C-73 and C-74	33
9	Elemental Analysis of Impurities	38
10	Impurity Content from Elemental Analysis	39
11	Activity and Isotopic Analysis	40
A1.1	^{137}Cs Decay Chain Data	A-11
A1.2	WESF Capsule Gamma-Ray Emission Spectrum	A-15
A1.3	WESF Capsule Radiation Emission Data	A-17
A1.4	WESF Capsule Energy Deposition Profile From CYLTRAN	A-18
A1.5	^{137}Cs Decay Data	A-19
A1.6	^{137}Cs Decay Data and Energy Deposition Probabilities	A-20
A1.7	Energy Depositions Per ^{137}Cs Decay; 0.095-in Wall Thickness	A-20

1. INTRODUCTION

Sandia National Laboratories, Albuquerque (SNLA) has been conducting research on the use of gamma irradiation for sterilization and disinfection purposes since the mid-1960s. In 1979, a pilot-scale irradiator, the Sandia Irradiator for Dried Sewage Solids (SIDSS),* went on line. The radiation source consisted of 15 Waste Encapsulation and Storage Facility (WESF) capsules, each initially containing approximately 68 kCi of cesium-137. The capsules were mounted horizontally on the plaque in a linear array with 1.375 inches between capsules. The source operated in an air environment with 300 ft^3/min (100 linear ft/min) of prefiltered air flowing around the plaque and capsules.

Two heat transfer models have been used to calculate temperature profiles for the WESF capsules. A thermal analysis for the inner capsule temperatures based on the SIDSS plaque configuration and in situ temperatures was made by Jack Tills and Associates using a TAC2D thermal model (Appendix A). R. J. Shippell used the finite element code ANSYS to calculate temperature profiles based upon data obtained during thermal cycling studies performed at the Pacific Northwest Laboratory (PNL)** (Tingey et al., 1985).

The WESF capsules were designed for waste storage and were not registered as sealed radiation sources. The licensing of non-Department of Energy (DOE) facilities for use of the WESF capsules requires that the capsules be registered as sealed sources. The data required for registration of the WESF capsules includes analysis of the capsule integrity under normal and adverse conditions. The absence of data from the detailed examination of aged WESF capsules (in particular, those aged in dry environments) was noted by Kenna (1982). Therefore, SNLA proposed the periodic destructive analysis of aged WESF capsules from SIDSS. The first capsule (C-117) was removed from service for analysis and characterization in August 1981 after 2.3 years of service (Kenna and Schultz, 1983). In April 1984, two additional WESF capsules (C-73 and C-74) were removed after 5 years of service. Analysis of these capsules was a joint undertaking of SNLA and PNL with assistance from Rockwell Hanford Operations (RHO). This program emphasized metallographic studies of the inner capsule and inner capsule weld areas (remote weld) and analysis of the salt.

---

*M. E. Morris, Sandia Irradiator for Dried Sewage Solids, Sandia National Laboratories, Albuquerque, NM, SAND79-2240, July 1980.

**Operated for DOE under Contract DE-AC06-76RLO 1830 by Battelle Memorial Institute.

2. CAPSULE DATA AND HISTORY

The WESF capsule (Figure 1) consists of a pair of nested right circular cylinders fabricated from Type 316L stainless steel (SS) (see Appendix B for material specification). The capsule was initially designed for storage of cesium-137 removed during the processing of defense nuclear fuel. The recovered cesium is purified and converted to the chloride. The chloride is melt-cast into the inner capsule and fitted with an O-ring (Type 316L SS), an O-ring retainer (Type 316L SS), a helium-saturated disk, and a tungsten inert gas (TIG) cap remotely welded. The inner capsule is decontaminated, and the weld integrity is checked. It is then placed and sealed into the outer capsule. The outer capsule weld integrity is checked and the finished capsule is decontaminated.

Capsules C-73, C-74, and C-117 were fabricated at WESF, Hanford, Washington, from September 12 to 26, 1975. Table 1 gives the pertinent data and historical calendar for the capsules.

After approximately 30 months of use in the SIDSS irradiator, tests were conducted to verify the lack of contamination on the outer surfaces of a capsule in the irradiator plaque. In March and October 1982, swipe tests were made on one of the WESF cesium chloride capsules while in the operating position. The SNLA Health Physics Counting Laboratory reported no trace of cesium-137 on any of the swipes.

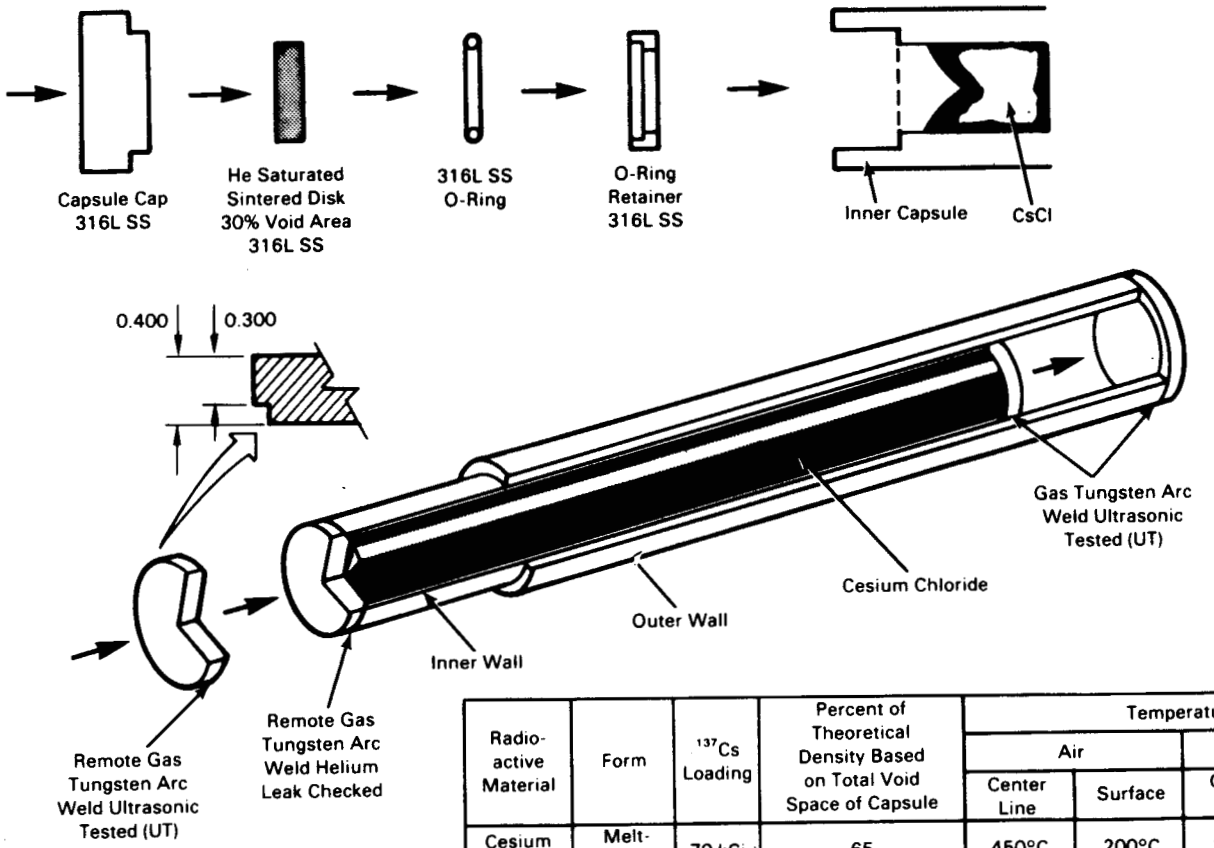

Radio-active Material	Form	^{137}Cs Loading	Percent of Theoretical Density Based on Total Void Space of Capsule	Temperature			
				Air		Water	
				Center Line	Surface	Center Line	Surface
Cesium Chloride	Melt-Cast	70 kCi	65	450°C	200°C	327°C	58°C

Radio-active Material	Capsule									
	Inner					Outer				
	Material	Wall Thickness	Outside Diameter	Total Length	Total Cap Thickness	Material	Wall Thickness	Outside Diameter	Total Length	Total Cap Thickness
Cesium Chloride	316L Stainless Steel (UT)	0.095 (UT)	2.250	19.375	0.400	316L Stainless Steel (UT)	0.109 (UT)	2.625	20.425	0.400

Note: All Dimensions are in Inches

Figure 1. Detail of WESF Cesium-137 Source Capsule

Table 1

Historical Data for WESF Capsules

	Capsule		
	C-73	C-74	C-117
Fabrication date	9/10/75	9/12/75	9/26/75
Net weight of salt, kg	2.84	2.83	2.70
Activity, kCi			
Calorimetry 9/75	68.7	68.5	63.7
Calorimetry 4/84	53.5	55.2	
Radiometry 11/81			60.1[a]
Radiometry 12/84	54.5	59.7	
Shipped to SNLA	7/28/78	7/28/78	8/18/78
Stored in cobalt pool (wet storage)	8/78 - 4/79	8/78 - 4/79	8/78 - 4/79
Transferred to SIDSS	4/23-24/79	4/23-24/79	4/23-24/79
Air environment, 300 ft^3/min	4/30/79	4/30/79	4/30/79
Removed from service	4/11/84	4/11/84	8/81
Total life, yr	8.6	8.6	5.9
Water storage, yr	3.6	3.6	3.6
Service life, yr	5.0	5.0	2.3

[a] Calculated based on radiometric analysis (11/20/81) 22.2 Ci/g (Kenna and Schultz, 1983, 22.2 x 2.708 = 60.1 kCi).

3. CAPSULE DISASSEMBLY AND SAMPLE PROCUREMENT

Capsule examination, disassembly, and sampling were done at WESF by RHO with SNLA and PNL observers. On receipt of the shipping cask, the two capsules, C-73 and C-74, were transferred into the WESF shielded (hot) cells and identified. The total activity within each capsule was determined calorimetrically (Table 1). On completion of the calorimetric measurements, the capsules were transferred into E-Cell for visual examination before disassembly. Multiple scratches, forming a pair of rings were observed on each of the outer capsules. The spacing between these markings indicated that the scratches were the result of contact between the capsules and the shipping rack during transit. Small localized area of discoloration were discovered on the "hot end"* caps and sides of both capsules. On the C-74 capsule, the discolored area was a circle with a diameter of approximately 0.375 in (9.5 mm). All discoloration was judged to be of external origin, i.e., possibly oil from the SIDSS shutter mechanism. There was no evidence of pitting or corrosion on the outer capsules.

When the inner capsules were removed from their respective outer containment, the caps and all surfaces were shiny with no discolored areas. The interior walls of the outer capsules were also shiny with no discernible evidence of discoloration.

Figure 2 is a line drawing of the typical cutting schedule followed for the disassembly of the capsules. All cutting started at the hot end, identified by the letter "C" preceding the capsule number on the cap.

The order of operations was:

- Cut hot end off outer capsule.
- Remove inner capsule.
- Cut hot end off inner capsule.
- Cut inner capsule into thirds. (The notches are sample identifiers.)
- Obtain and package salt samples.
- Dissolve remaining salt from sample rings.
- Cut and split notched sample rings.
- Package split rings, cap halves, and solid salt samples for transfer to PNL.
- Repeat all steps except dissolution of salts for outer capsule.
- Cut hot-end cap and cold-end cap of inner capsule in half.

All work was completed on the first capsule before beginning work on the second capsule.

---

*The reference to "hot end" indicates the end welded in the Hot Cell and is not a reference to a thermal condition.

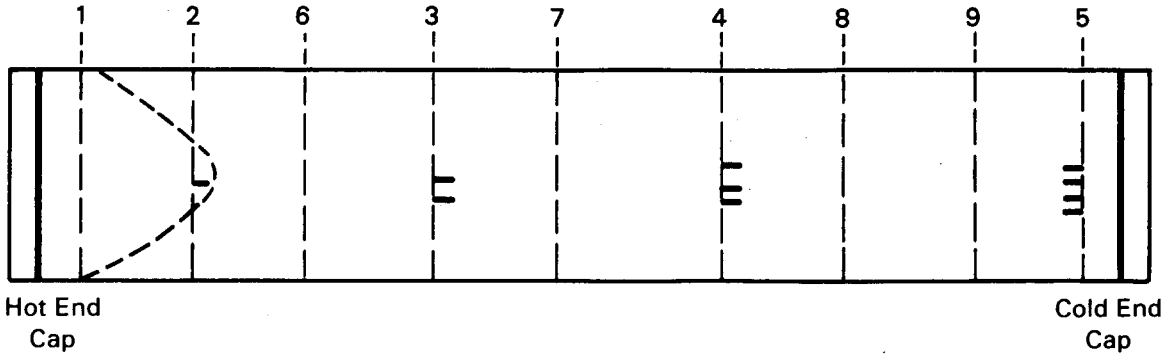

Figure 2. Typical Cutting Schedule. Numbers indicate the sequence of cuts. (- Notches, sample identification)

Samples of the salt were scraped from each of the notched cut surfaces and loaded into marked containers (bullets). The cast salt was very hard, making it difficult to obtain samples.

Figures 3 through 8 are photographs of the as-cut surfaces prior to salt sampling. Figure 3 is a photograph of the hot-end weld and a portion of the inner capsule prior to the start of disassembly Figure 4 shows the salt depth and shrinkage void after the first cut (which removed the cap), sintered disk, O-ring, and retainer. Figure 5 shows the surface of the salt and the bottom of the shrinkage hole. This is the sample with one notch. The dark coloration in the shrinkage void (bottom center of capsule) is also discernible at the center of all cut surfaces and may be due to the concentration of impurities during the solidification process. Figures 6, 7, and 8 show the surfaces of the samples identified by two, three, and four notches.

After the initial cutting, notching, and salt sampling, the cut pieces were immersed in a large (3-gal) container of water. During the process of dissolution, there was some gas evolution with the formation of a semisolid porous mass (Figure 9). Observations made during dissolution of the 47 WESF cesium chloride capsules in a previous study revealed that only two capsules had shown any evidence of gas generation (Tingey, Wheelwright, and Lytle, 1984). The gas generation may indicate that a small fraction of the salt in these two SIDSS capsules remained in a chemically reactive form.

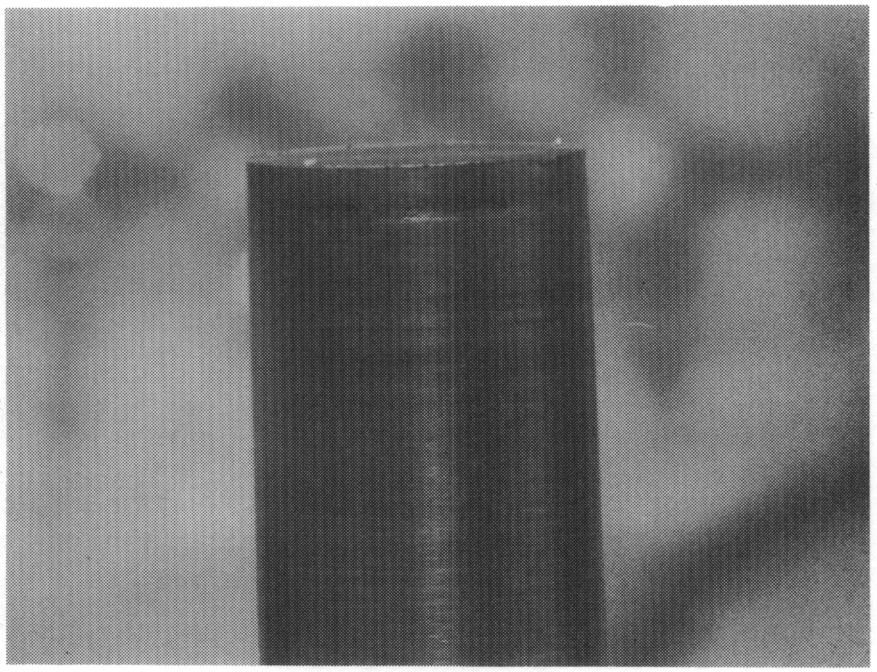

Figure 3. Hot-End Weld and Inner Capsule

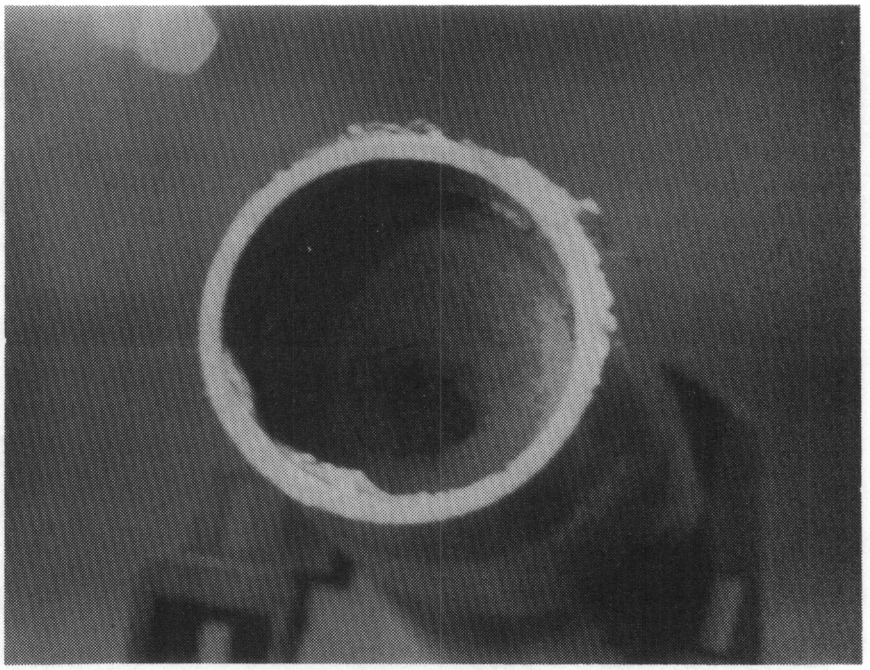

Figure 4. Depth of Salt from End Cap After First Cut

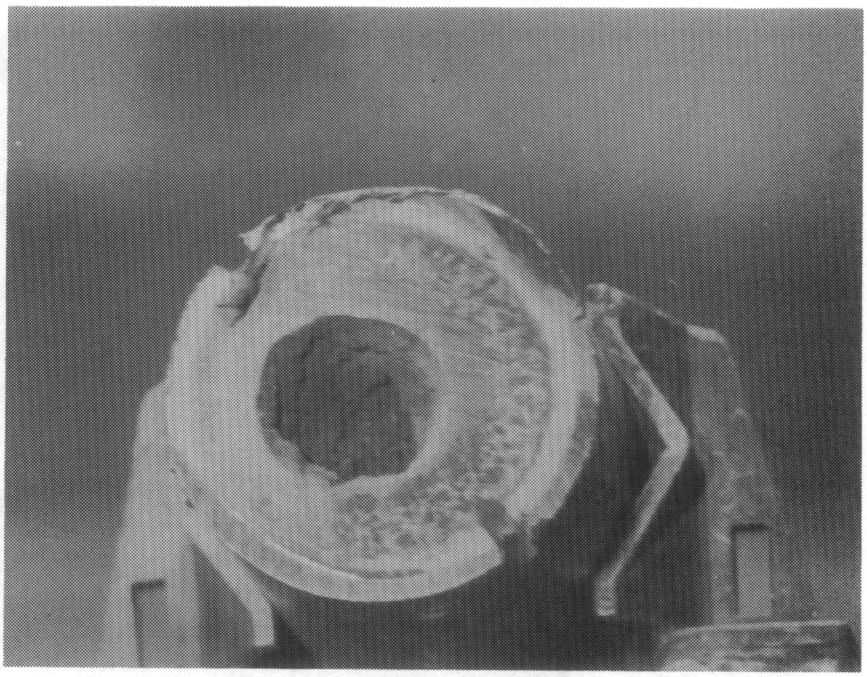

Figure 5. Surface of Salt and the Bottom of Shrinkage Hole at the One-Notch Location

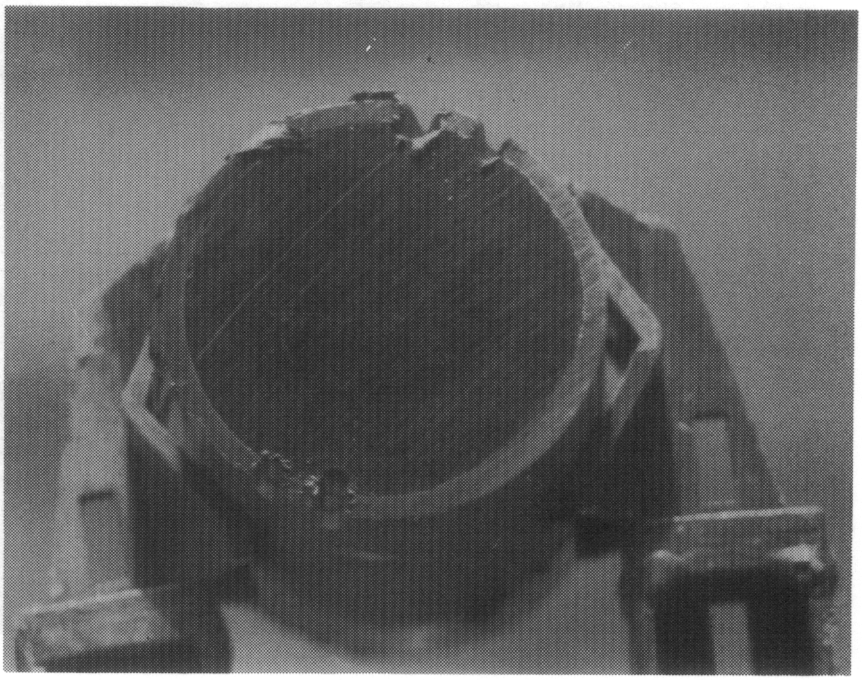

Figure 6. Surface of Salt at the Two-Notch Location

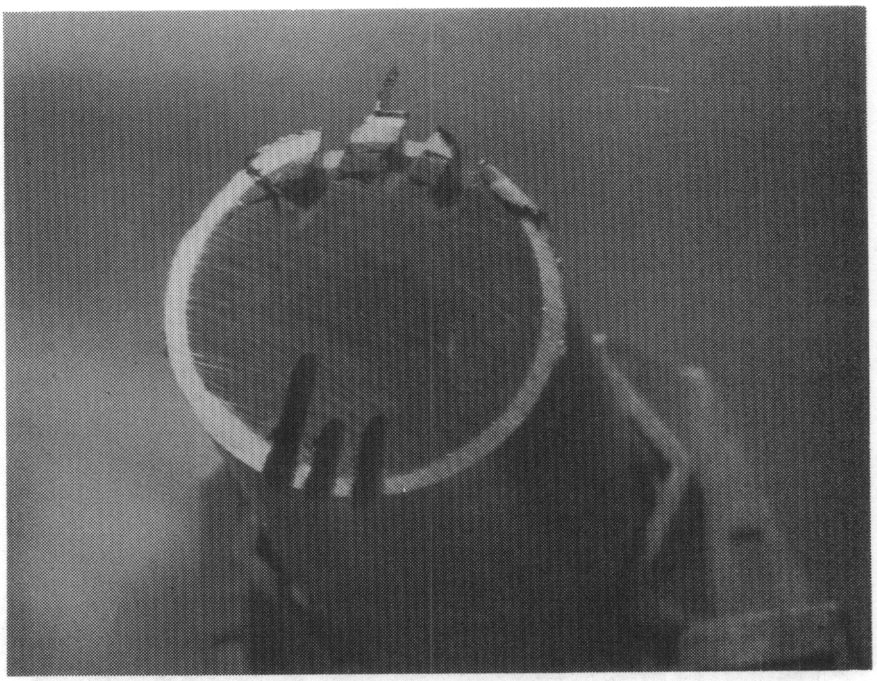

Figure 7. Surface of Salt at the Three-Notch Location

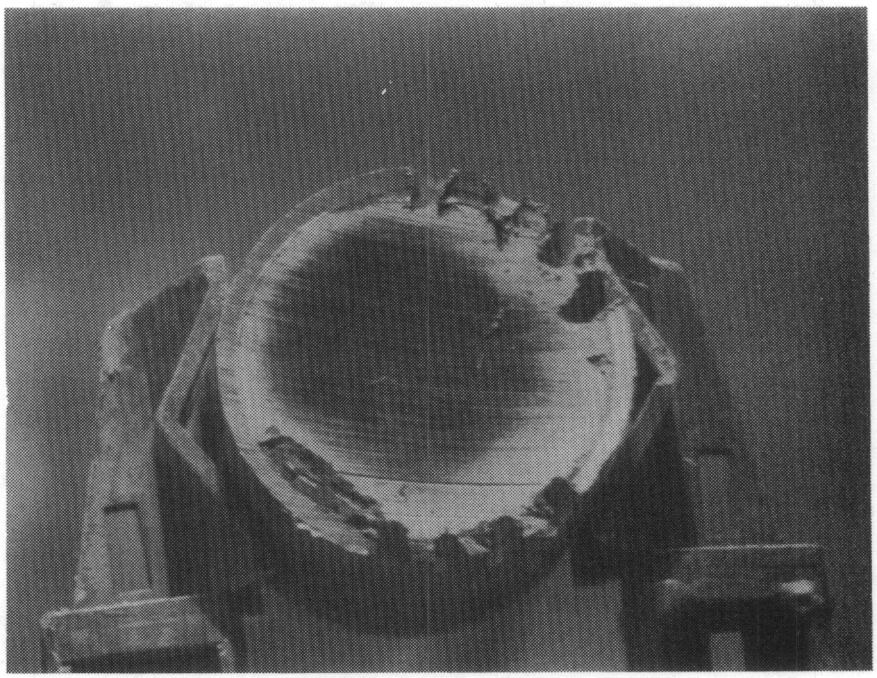

Figure 8. Surface of Salt at the Four-Notch Location

Figure 9. Buoyant Mass During Dissolution

4. SHIPPING CAPSULE CUTTING AND MATERIAL INVENTORY

Four shipping capsules containing the inner and outer half-rings from capsules C-73 and C-74 and the eight salt samples were transferred to the PNL hot cell facility in Building 324. Table 2 identifies the shipping capsules and the packaged contents list. The capsules were opened using a lathe and a parting tool to cut off the end cap. Capsule 1821 was opened first. After removing the end cap, the shipping capsule was tilted over the hot cell work table. At this time, it was detected that two of the salt bullet caps were off. A closer examination revealed that the bulk of the CsCl salt that had been in the bullets was distributed throughout the shipping capsule. An attempt was made to recover some of this material, noting the potential for cross contamination and introduction of extraneous impurities. Capsule 1821 also contained seven half-rings (one half-ring from ring 1 was missing) and two end cap halves.

Capsule 1814 was then opened using the same lathe method. A clean receiving tray was prepared in case any of the salt bullets were open in this capsule. The tray was used to reduce the amount of impurities that would be introduced when recovering any uncontained salt material. When the capsule was emptied into the tray, all four of the salt bullets were open. The loose salt was collected and saved, noting that the material could have been contaminated. Capsule 1814 also contained seven half-rings (one half-ring from ring 4 was missing) and two end-cap halves.

The eight original salt bullets were recapped. The two composite salt samples and the eight bullets were sent to the PNL hot cell in Building 325 for preparation of solutions for chemical and isotopic analyses.

Table 2

WESF Capsule Identification and Capsule Contents

Contents of Capsule 1814	Contents of Capsule 1821	Contents of Capsule 1823	Contents of Capsule 1829
Capsule C-73 inner rings	Capsule C-74 inner rings	Capsule C-74 outer rings	Capsule C-73 outer rings
Capsule C-73 inner end cap	Capsule C-74 inner end cap	Capsule C-74 outer end cap	Capsule C-73 outer end cap
4 salt bullets from C-73	4 salt bullets from C-74		

5. MACRO EXAMINATION AND MECHANICAL THICKNESS MEASUREMENTS

The half-rings from capsules 1814 and 1821 were examined in the hot cell using a Kollmorgen periscope. Since the rings had been exposed to the loose salt from the open sample bullets in the shipping capsule, there was particulate adhering to the surfaces of interest. The sections were then washed in deionized water in an ultrasonic bath to remove the particulate. During this cleaning process, the wash solution developed a slight red tint due to suspended material. The rings were reexamined; all of the particulate had been removed. The inside surfaces of the rings were discolored to varying degrees except ring 4 of capsule C-74 which had the brightest surface; ring 4 of capsule C-73 also had the brightest surface of the rings from that capsule.

An attempt was made to dissolve the particulate suspended in the rinse solution. Hydrochloric acid was added to an aliquot of the rinse solution in 1 percent concentration steps up to a total concentration of 10 percent acid. The particulate did not dissolve. It has been suggested by RHO personnel that the source of this particulate may be the entrained ion exchange resins used in the final stages of the cesium separation and purification process.

Each ring had been slit in half, and each half was notched for identification. The half-rings were then examined for selection of the metallographic sample. The areas that appear more corroded as judged by discoloration or surface marks were selected for metallographic examination (indicated by the ink markings in Figures 13 through 17). In addition, sections from each in-cell weld on the end caps and a bottom weld on capsule C-74 were selected for metallographic examination.

The half-rings were then recleaned in deionized water in an ultrasonic bath and removed from the hot cell. The radiation levels were low enough that subsequent work could be performed in an open front hood using forceps and lead-lined gloves. The remaining work included mechanically measuring the wall thickness, photographing the half-rings, and cutting the metallographic samples.

The thickness of each half-ring was measured mechanically at five equally spaced points* using a Microdot measurement head with a remote readout device. The detection head and anvil plate are shown in Figure 10. The method for measuring the thicknesses involved holding the half-ring with forceps and placing the outside diameter (OD) on the anvil. The detection head was lowered to contact the inside diameter (ID) surface. The minimum thickness was found, and then the detection head was raised. The half-ring was then rotated to the next position, and the process

---

*An occasional adjustment of position or no reading was due to severe damage to the wall by the notching device.

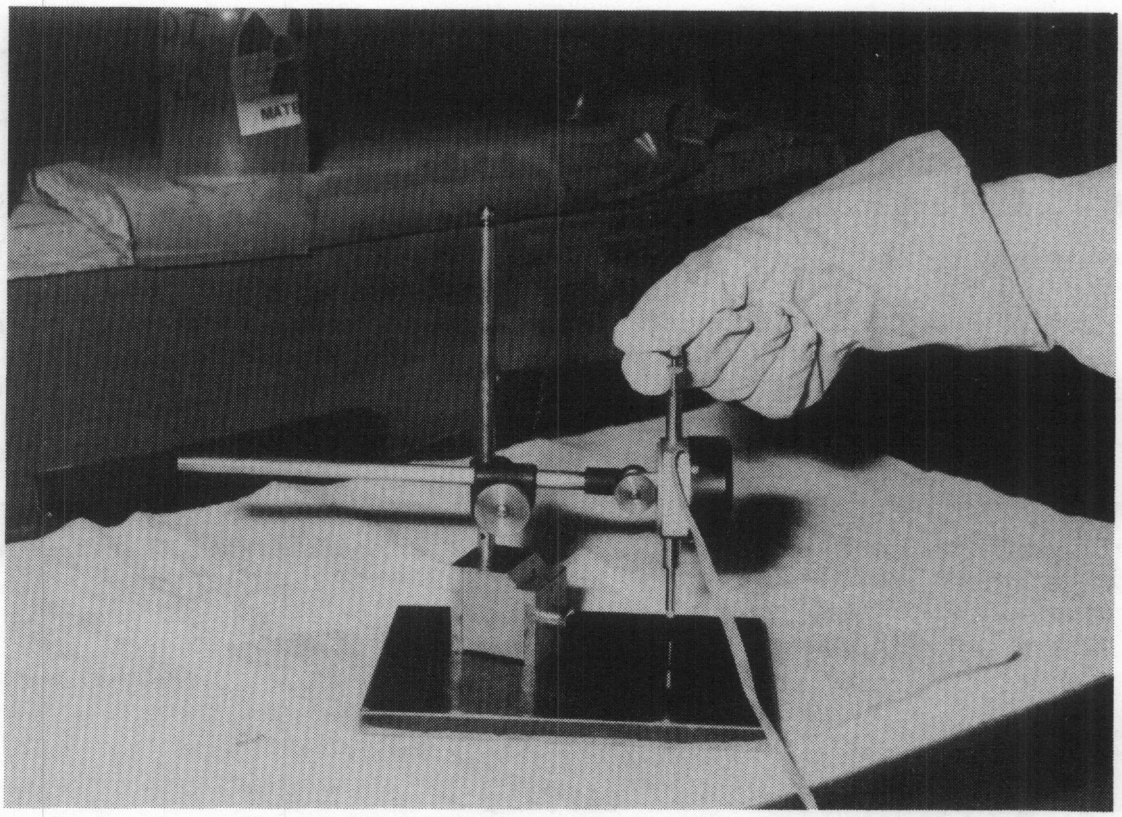

Figure 10. Detection Head and Anvil Plate

was repeated. The results for capsules C-73 and C-74 are shown in Tables 3 and 4, respectively; plots of the thickness data for capsules C-73 and C-74 are shown in Figures 11 and 12, respectively. The circumferential position numbers are arbitrary when comparing ring to ring because there was no way to correlate the individual half-rings from one vertical position to the next. In addition to the circumferential thickness measurements, the center thickness of each metallographic section was measured (Table 5). Two measured gauge blocks were obtained from the standards laboratory to check the measurement equipment. The standard values and the measured values are given in Table 6.

Each half-ring was then photographed. Figures 13 through 20 show photographs that were taken of the ID wall from each ring. Note the bright appearance of ring 4 of capsule C-74 and the machine-like markings on the surface.

Table 3

Circumferential Thickness Measurements for Capsule C-73[a]

	Thickness Measurements at 10 Circumferential Positions (in)									
Ring	1	2	3	4	5	6	7	8	9	10
1	0.095	0.094	0.093	0.094	0.093	[b]	[b]	[b]	[b]	[b]
2	0.094	0.094	0.095	0.096	0.096	0.094	0.094	0.094	0.094	0.094
3	0.091	0.091	0.092	0.091	0.093	0.092	0.092	0.091	0.091	0.091
4	0.091	0.092	0.091	[c]	0.090	0.091	0.092	[c]	0.091	0.091

[a]Per Specifications HWS-8835 Rev. 2, Appendix B, capsule wall thickness was 0.095 in ± 0.009 in.
[b]No data due to missing section.
[c]No data measurable due to surface damage from notching.

Table 4

Circumferential Thickness Measurements for Capsule C-74[a]

	Thickness Measurements at 10 Circumferential Positions (in)									
Ring	1	2	3	4	5	6	7	8	9	10
1	0.095	0.097	0.097	0.097	0.098	0.097	0.097	0.096	0.094	0.095
2	0.096	0.095	0.095	0.096	0.095	0.097	0.095	0.096	0.096	0.096
3	0.094	[b]	0.094	0.095	0.094	0.095	0.094	0.094	0.094	0.093
4	0.095	0.095	0.094	0.094	0.095	[c]	[c]	[c]	[c]	[c]

[a]Per Specifications HWS-8835 Rev. 2, Appendix B, capsule wall thickness was 0.095 in ± 0.009 in.
[b]No data measurable due to surface damage from notching
[c]No data due to missing section.

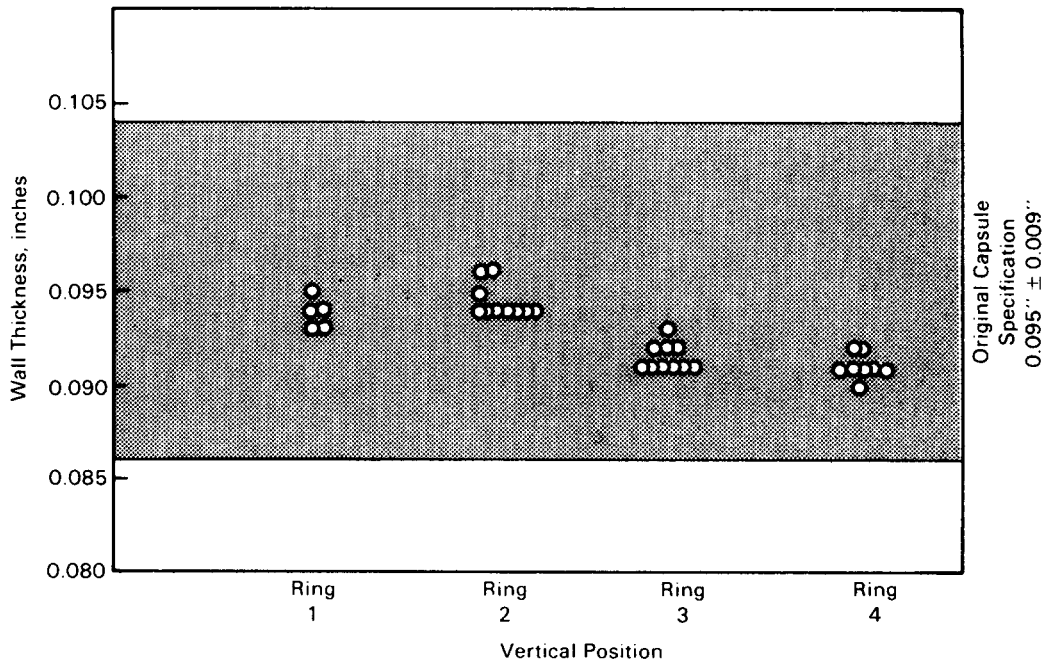

Figure 11. Capsule Wall Thickness Measurements for Capsule C-73

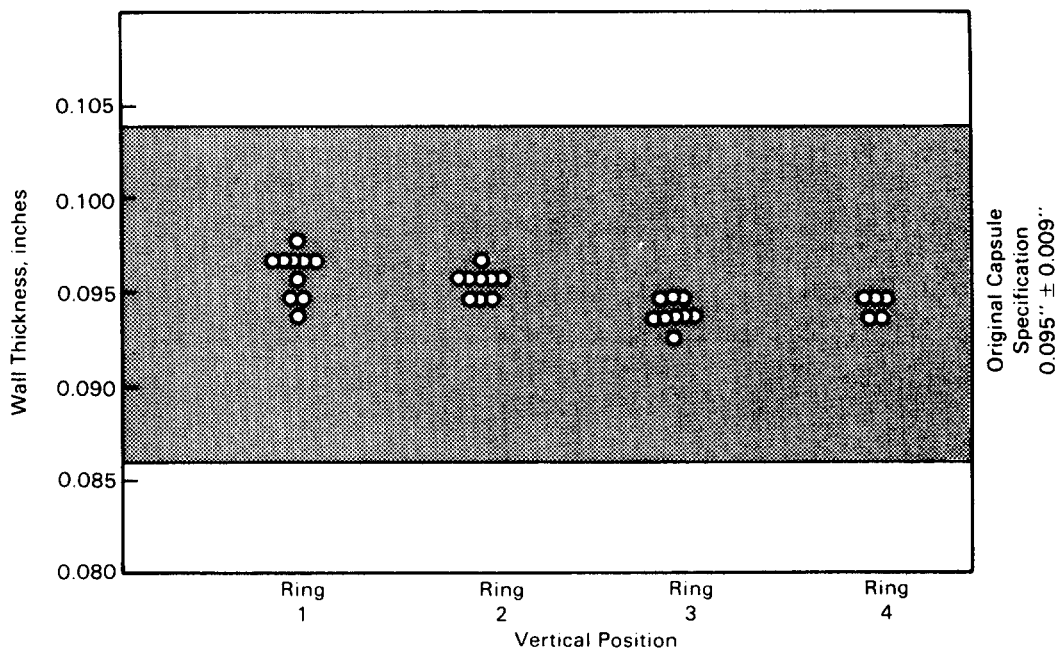

Figure 12. Capsule Wall Thickness Measurements for Capsule C-74

Table 5

Microdot Measurement of Metallographic Section

	Thickness (in)			
Capsule	Ring 1	Ring 2	Ring 3	Ring 4
C-73	0.094	0.094	0.094	0.091
C-74	0.094	0.096	0.094	0.095

Table 6

Standard and Measured Gauge Block Values

Gauge Block	Standard Value (in)	Measured Value (in)
1	0.1000	0.1002
2	0.1400	0.1404

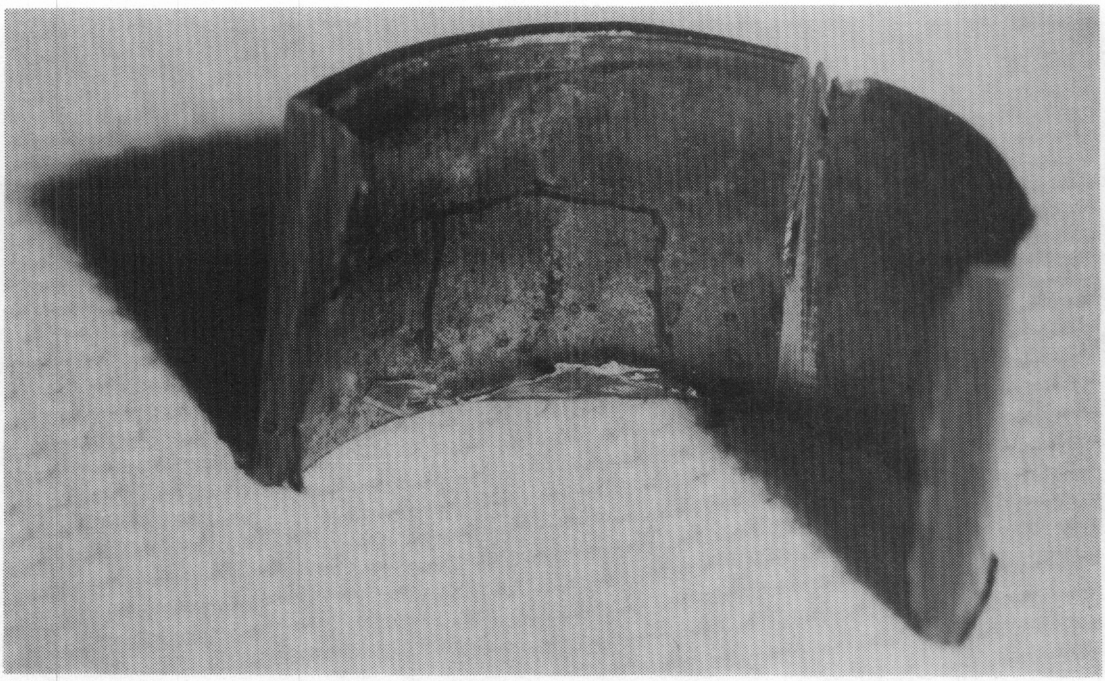

Figure 13. Capsule C-73, Ring 1

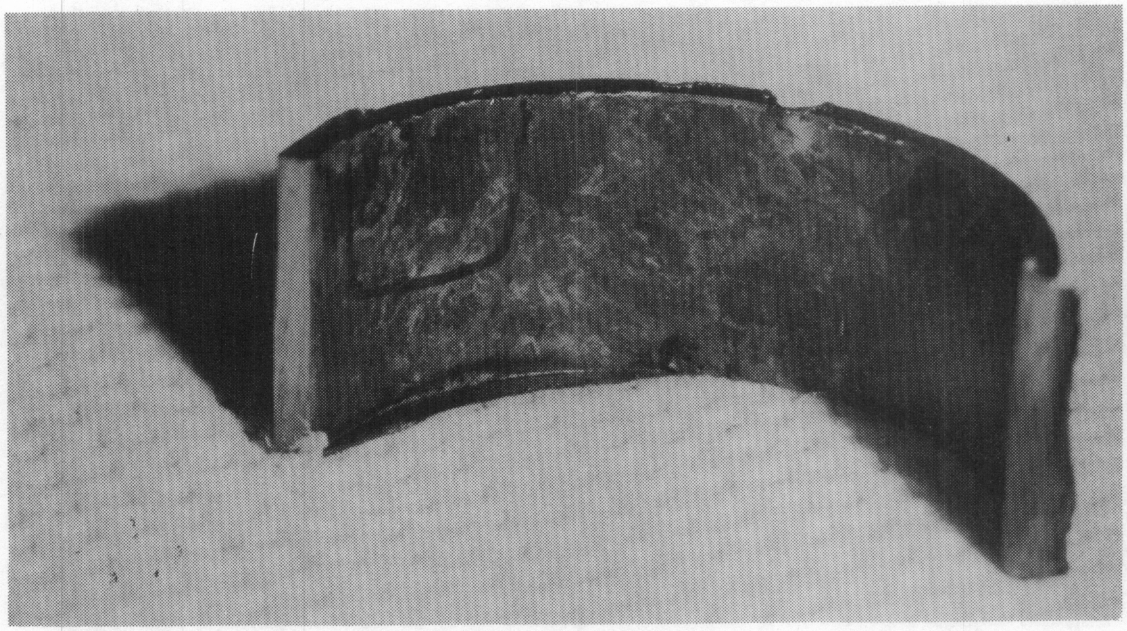

Figure 14. Capsule C-73, Ring 2

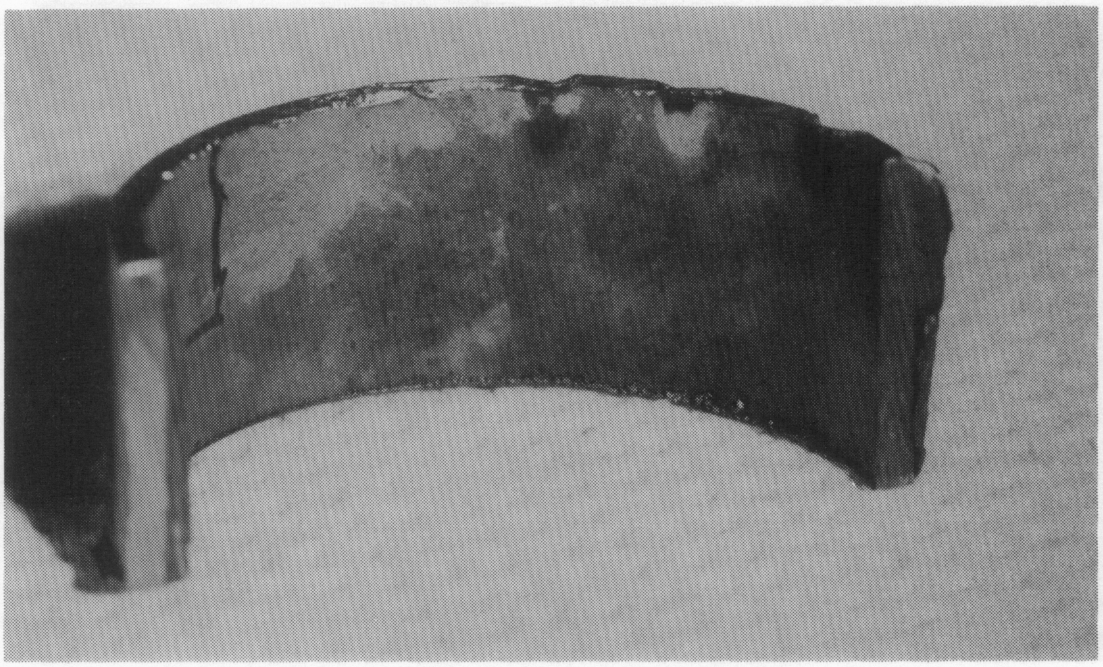

Figure 15. Capsule C-73, Ring 3

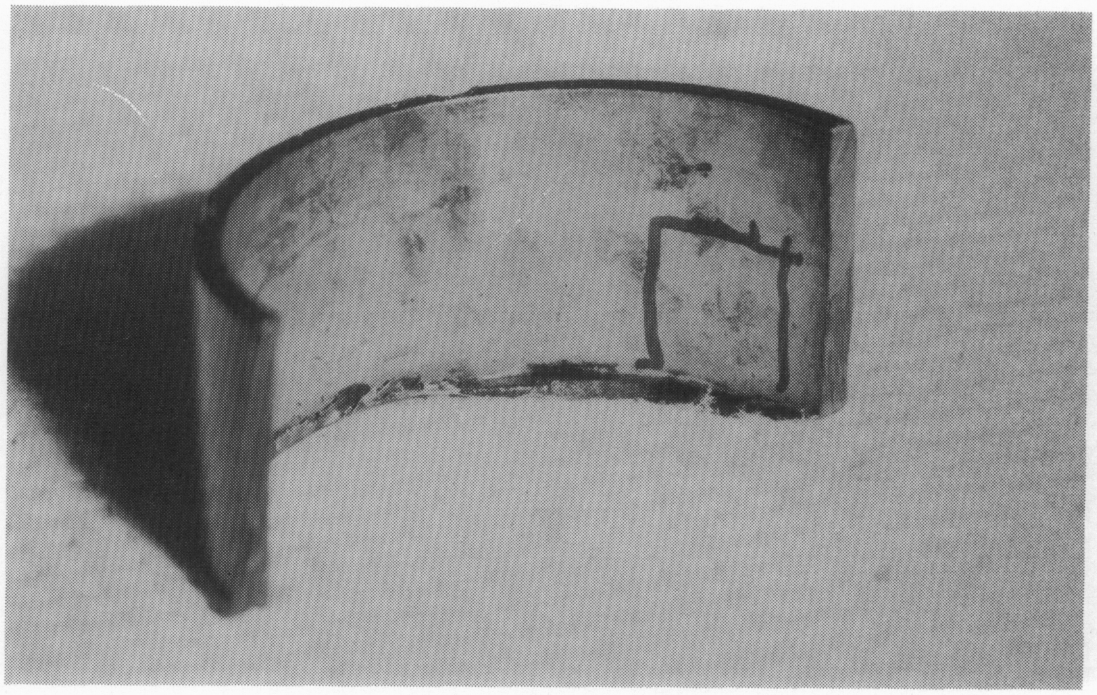

Figure 16. Capsule C-73, Ring 4

Figure 17. Capsule C-74, Ring 1

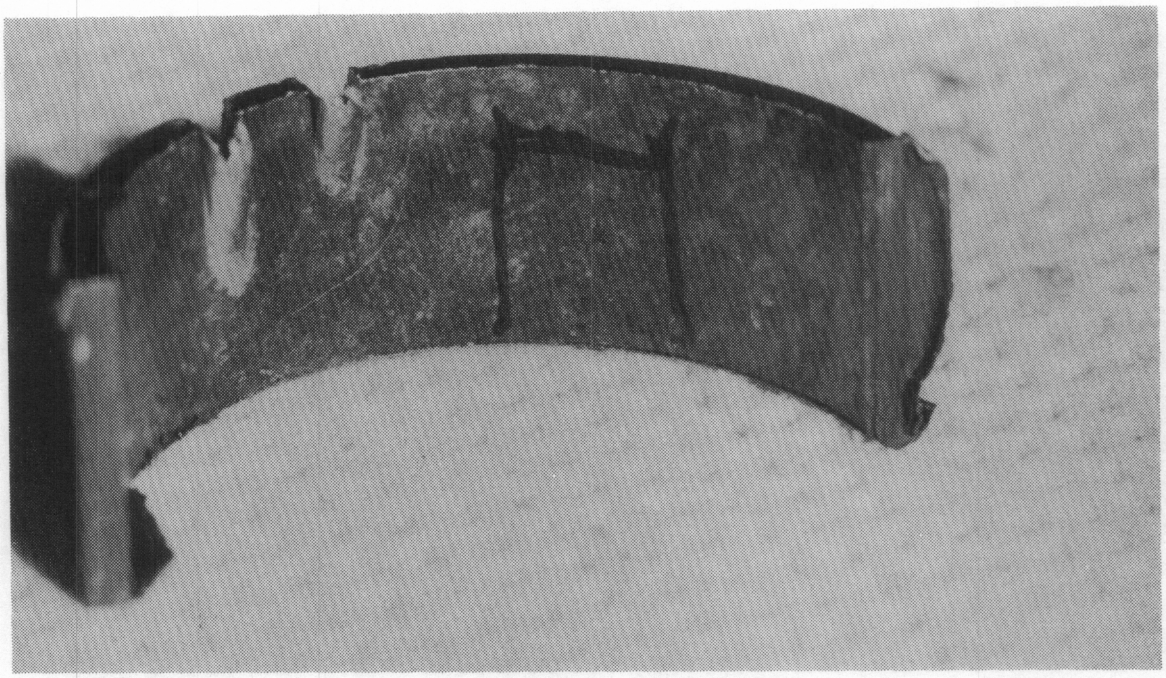

Figure 18. Capsule C-74, Ring 2

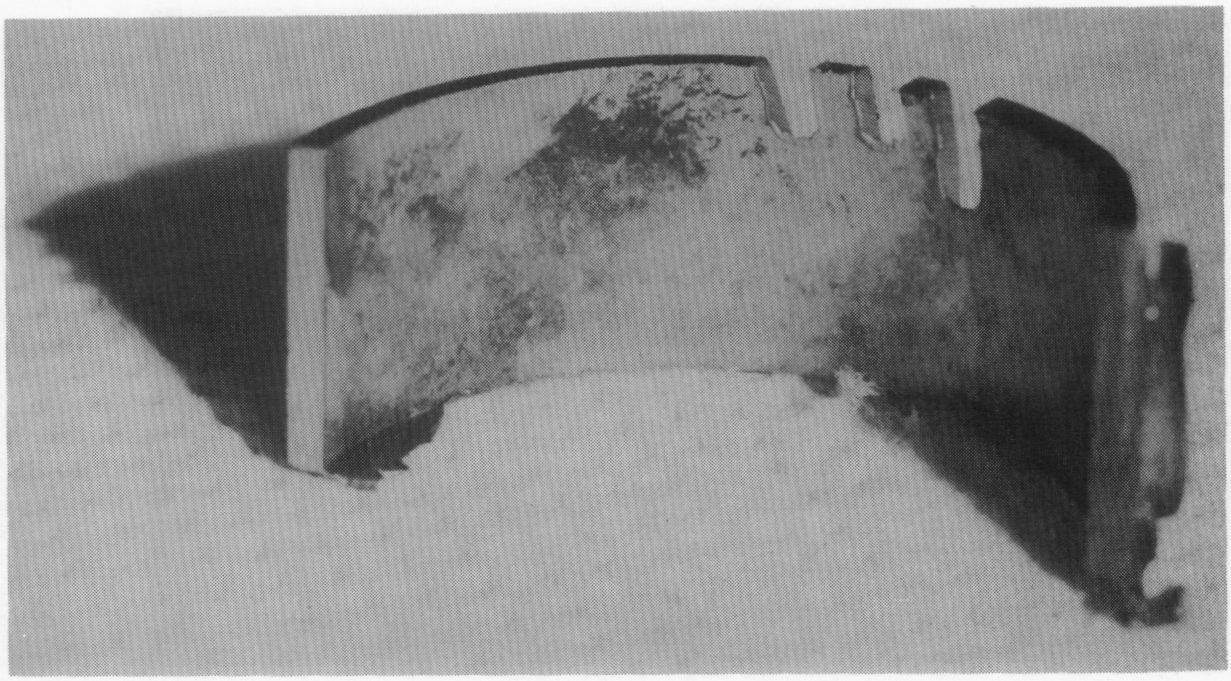

Figure 19. Capsule C-74, Ring 3

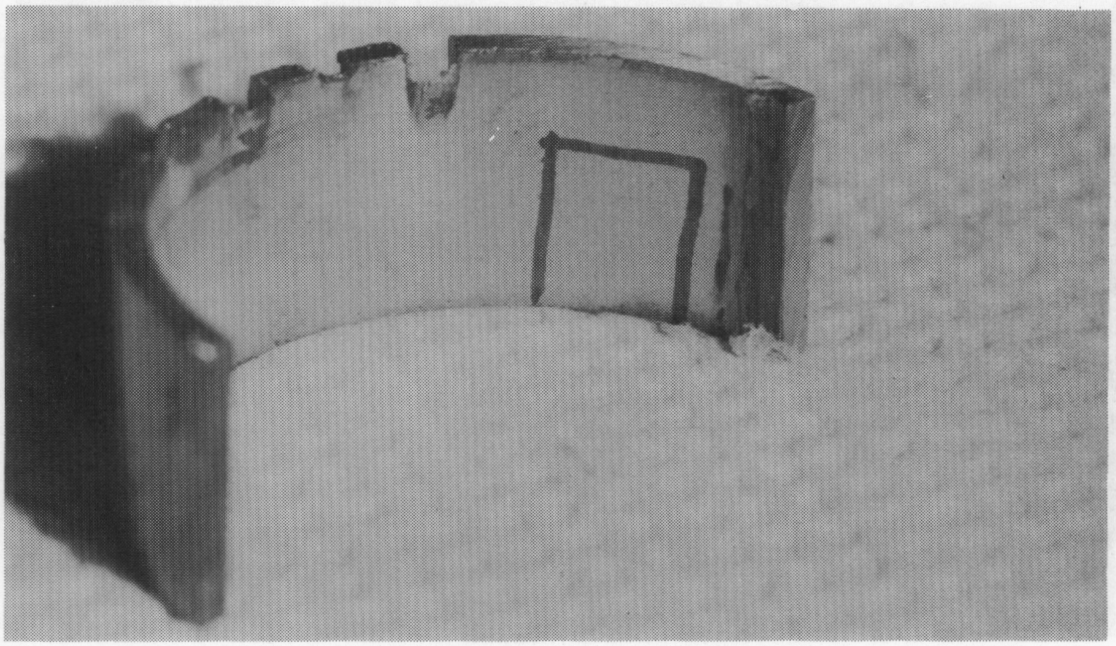

Figure 20. Capsule C-74, Ring 4

6. METALLOGRAPHY SPECIMEN SECTIONING AND EXAMINATION

Metallographic specimens obtained from the inner capsule of C-73 included one specimen from each ring location (total of four) and the (in-cell) weld. Metallographic specimens from capsule C-74 included one specimen from each of the four rings and both end welds. A Buhler Isomet low-speed diamond wafering saw was used to remove the sections. The wall sections were approximately 0.625 x 0.625 in and the weld samples were 0.5 x 0.5 in. These sections were transferred to the Hanford Engineering Development Laboratory (HEDL) postirradiation testing laboratory for metallographic preparation and examination. The four wall sections from each capsule were mounted together. Extreme care was used to insure perpendicularity of the sections with the polishing plane. The mounting method that was used is illustrated in Figure 21. The weld samples were mounted individually. After mounting in an epoxy resin, the samples were ground to the centerline and then polished with rotational polishing machines.

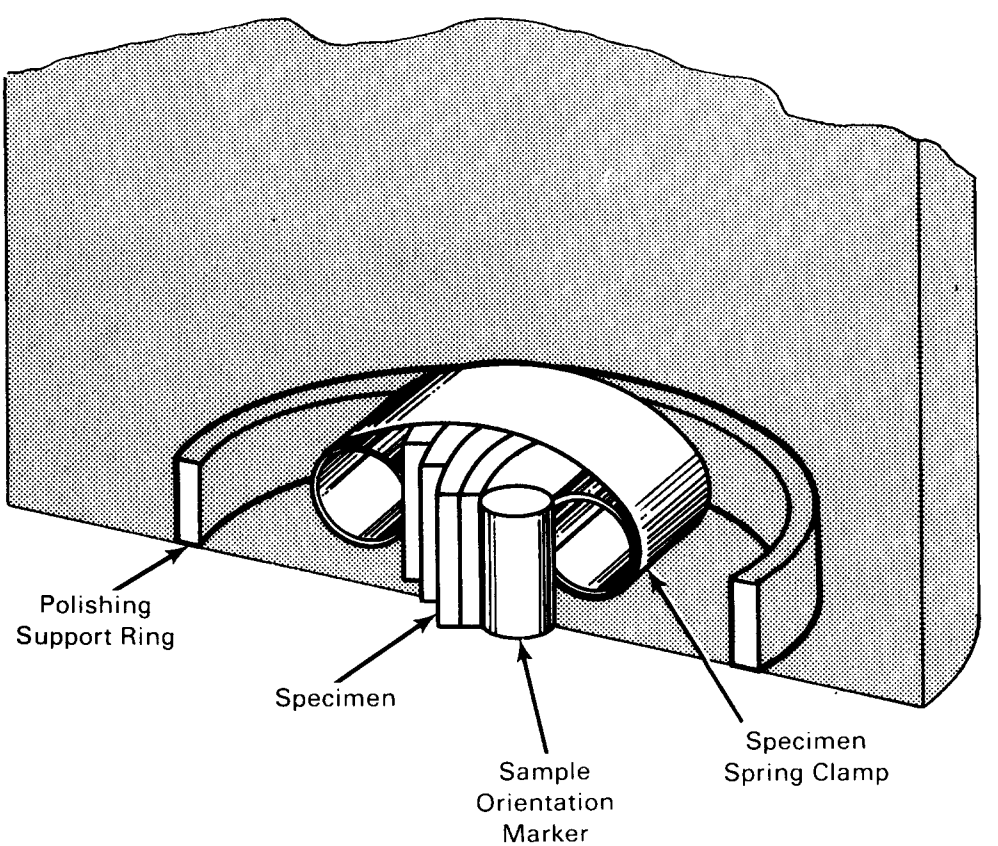

Figure 21. Metallographic Mounting Apparatus

All capsule wall samples were examined in an as-polished condition. Photomicrographs were taken of the wall sections at 50X and 225X. Representative micrographs from capsules C-73 (rings 2 and 3) and C-74 (rings 2 and 3) are shown in Figures 22 through 25.

All of the samples were etched for grain structure. An electrolytic etchant of 10 percent oxalic acid was used at a 5 Vdc potential. The etching time was based on grain boundary delineation and varied between 6 and 10 min. The wall sections were then reexamined and photomicrographs were taken at 36.5X, 50X, 225X, and 500X. The 225X and 500X photomicrographs were selected to document the areas of maximum irregularity on the ID surface. The etched weld photomicrographs at 25X are shown in Figures 26 through 28. Figures 29 through 32 are the photomicrographs of the etched samples at 50X, 225X, and 500X of rings 2 and 3 from both capsules. For comparison, two 500X photomicrographs taken of the zero-time capsule surface condition used in the ongoing Cesium Chloride Compatibility Testing Program (Bryan, 1985) are shown in Figure 33. Photomicrographs (500X) were also taken of the typical grain structure at the center of each all section (Figures 34 and 35).

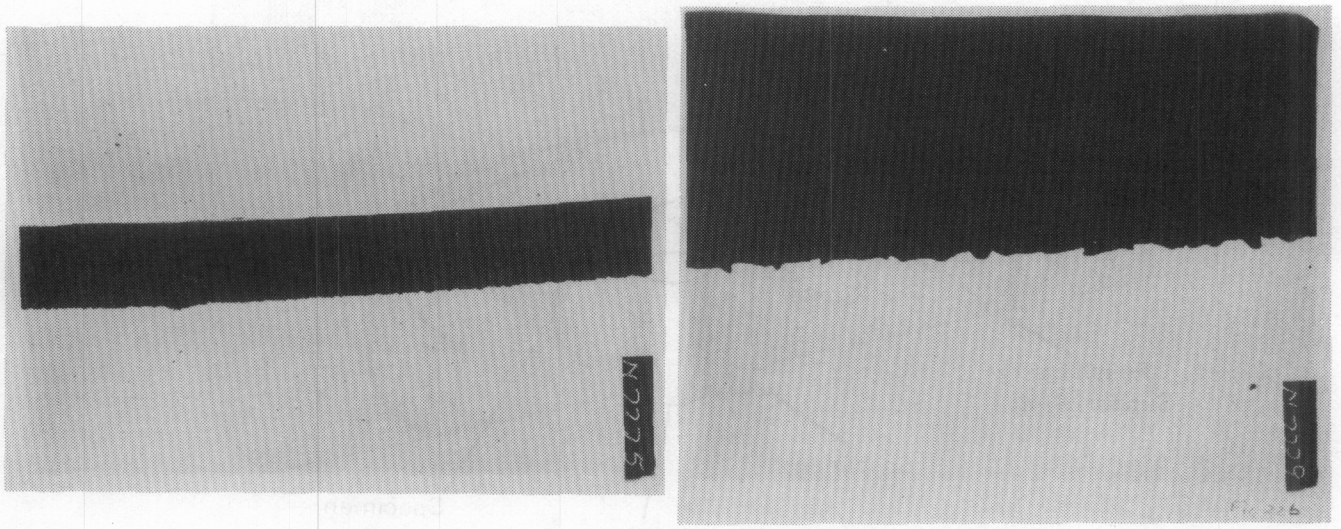

a. At 50X b. At 225X

Figure 22. Photomicrographs of Capsule C-73, Ring 2, As-Polished. (The light areas are metal; the dark areas are encapsulating compound.)

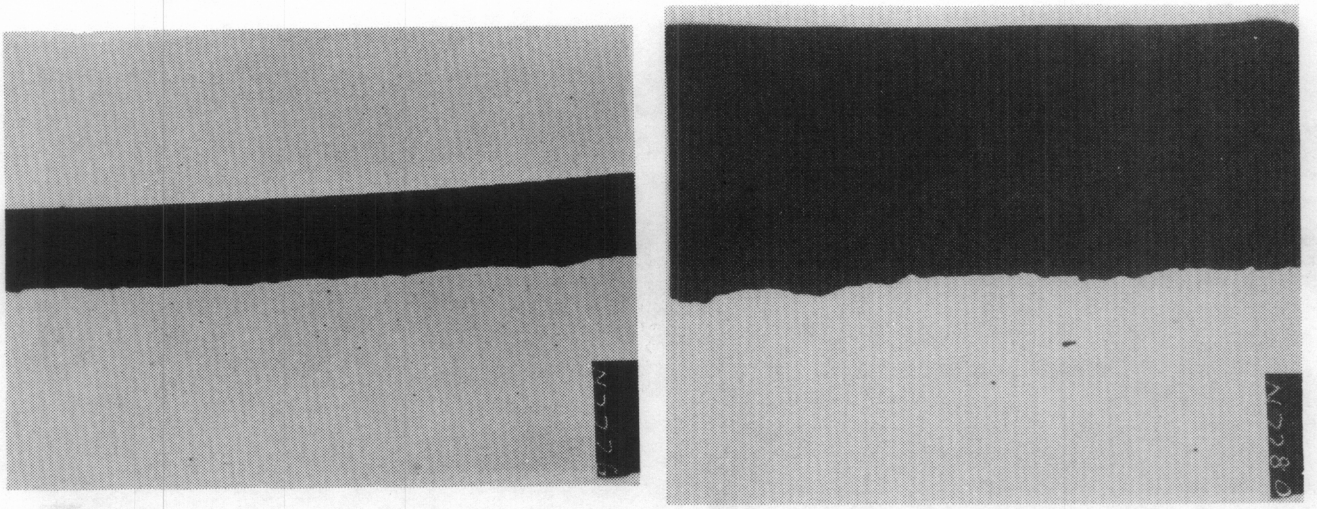

a. At 50X b. At 225X

Figure 23. Photomicrographs of Capsule C-73, Ring 3, As-Polished

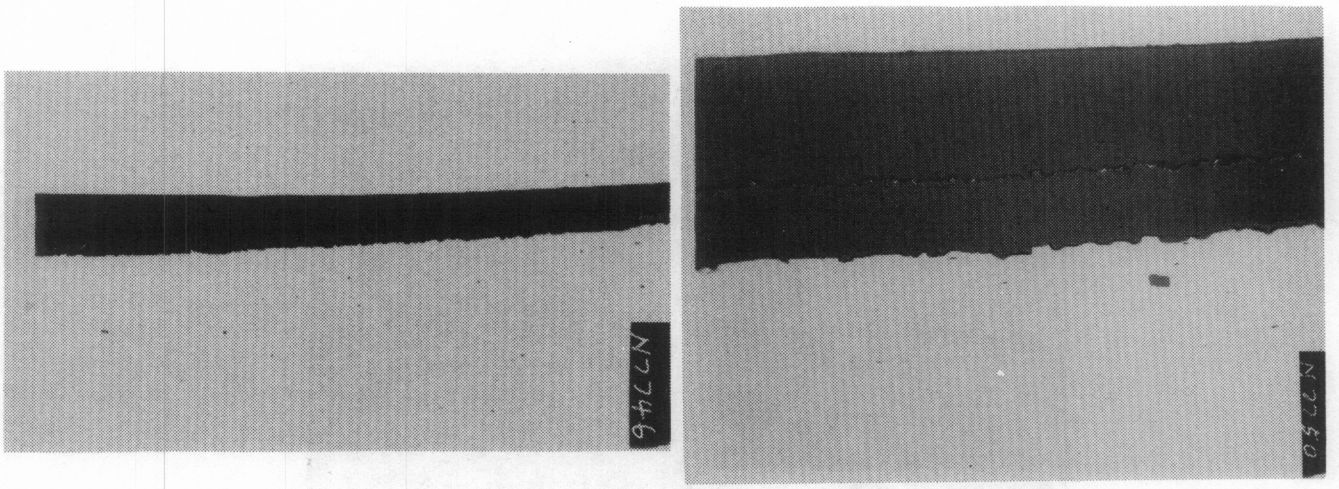

a. At 50X b. At 225X

Figure 24. Photomicrographs of Capsule C-74, Ring 2, As-Polished

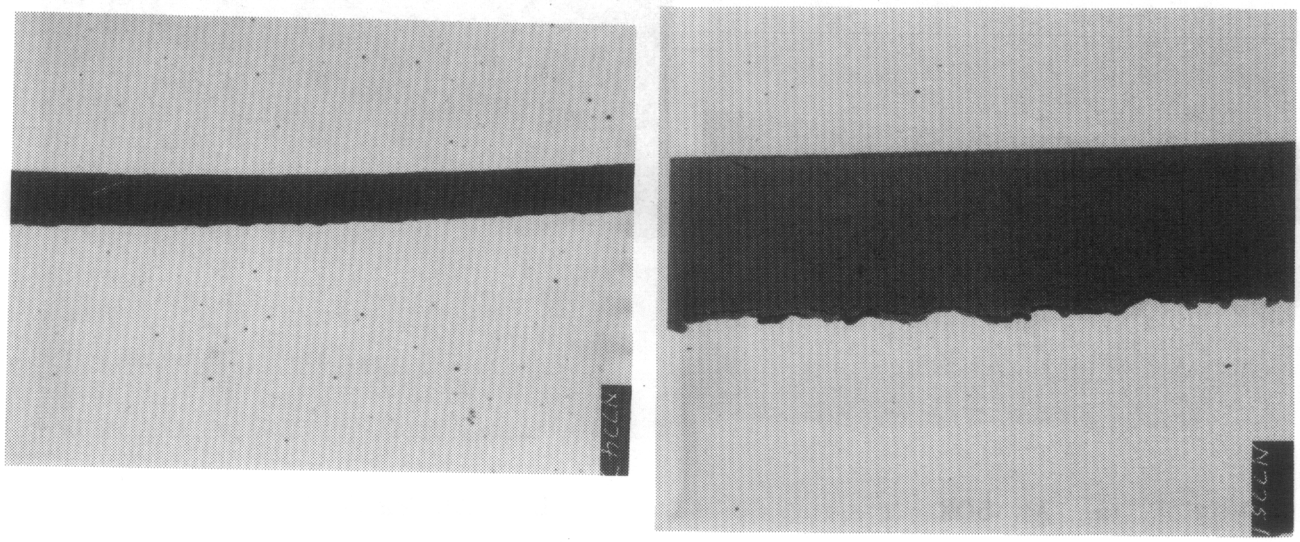

a. At 50X b. At 225X

Figure 25. Photomicrographs of Capsule C-74, Ring 3, As-Polished

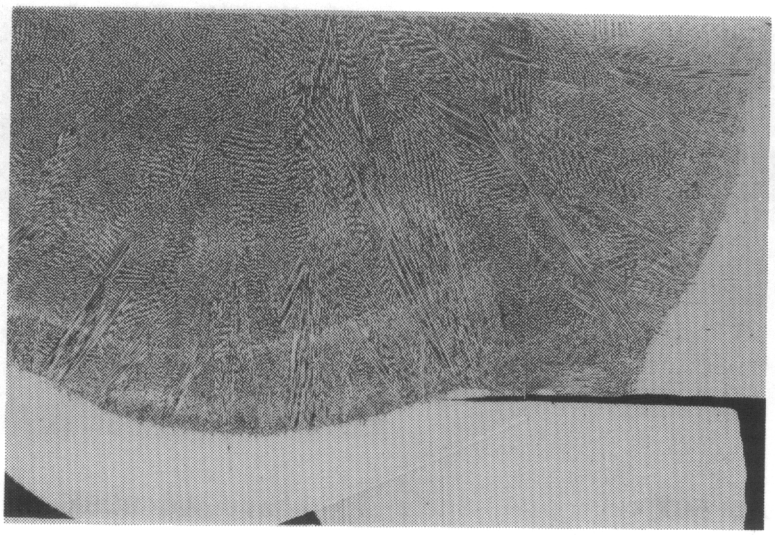

Figure 26. Photomicrograph of Capsule C-74 Top End-Cap Weld (In-Cell Weld)

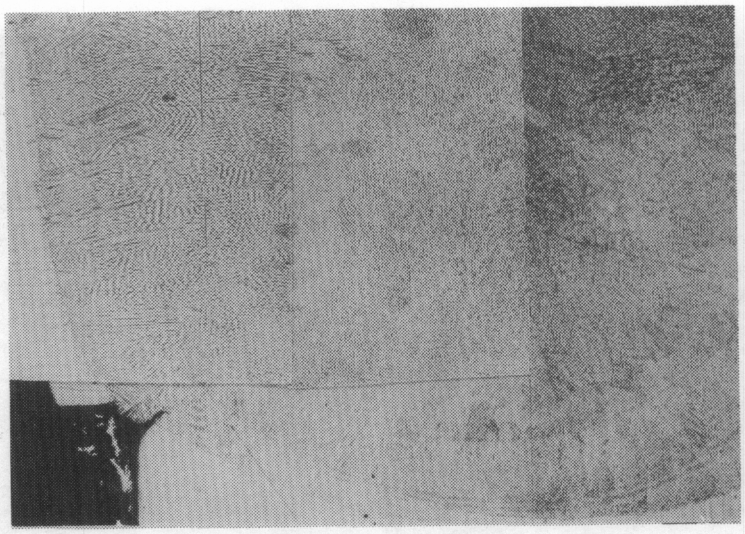

Figure 27. Photomicrograph of Capsule C-74 Bottom End-Cap Weld (Out-of-Cell Weld)

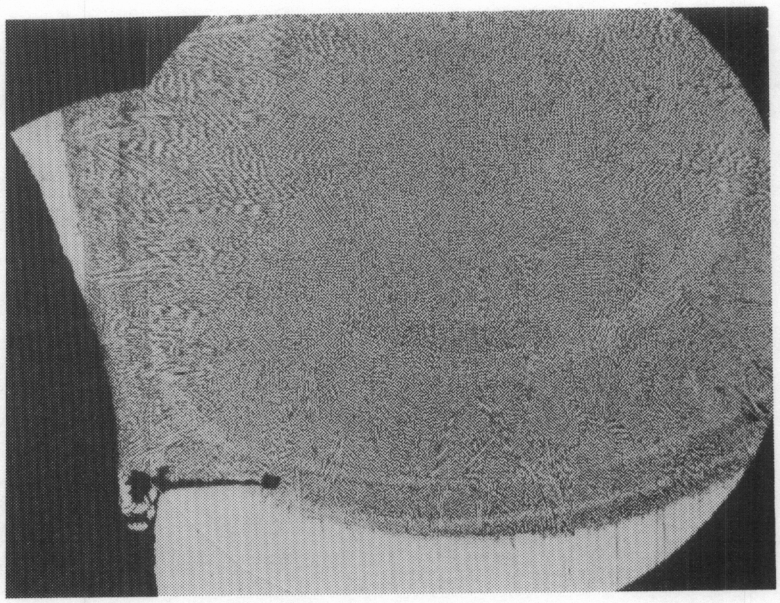

Figure 28. Photomicrograph of Capsule C-73 Top End-Cap Weld (In-Cell Weld)

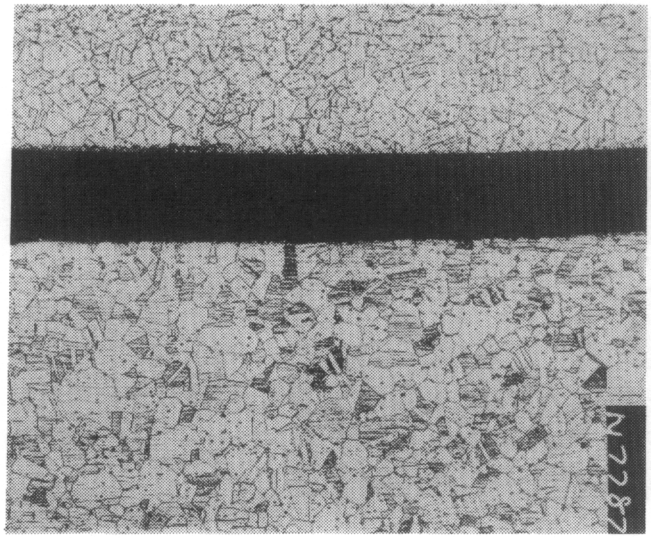

a. At 50X

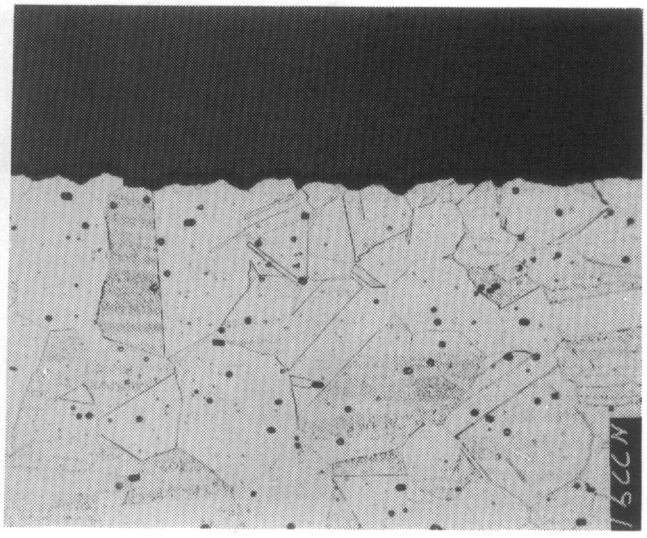

b. At 225X

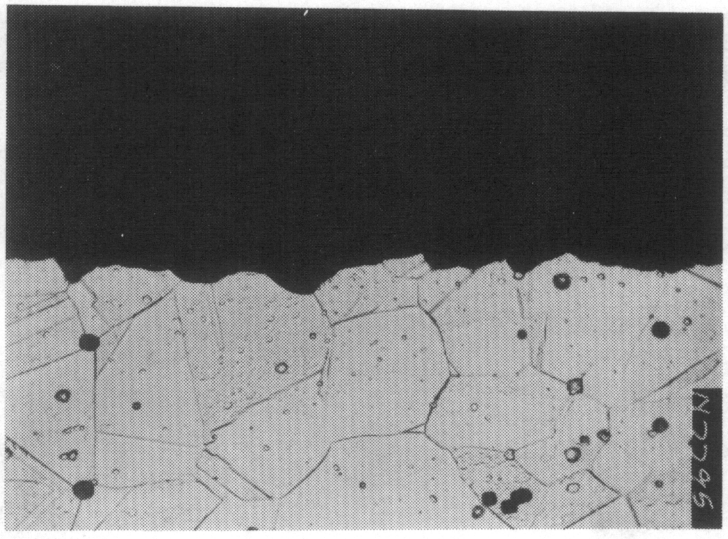

c. At 500X

Figure 29. Photomicrographs of Capsule C-73, Ring 2, Etched

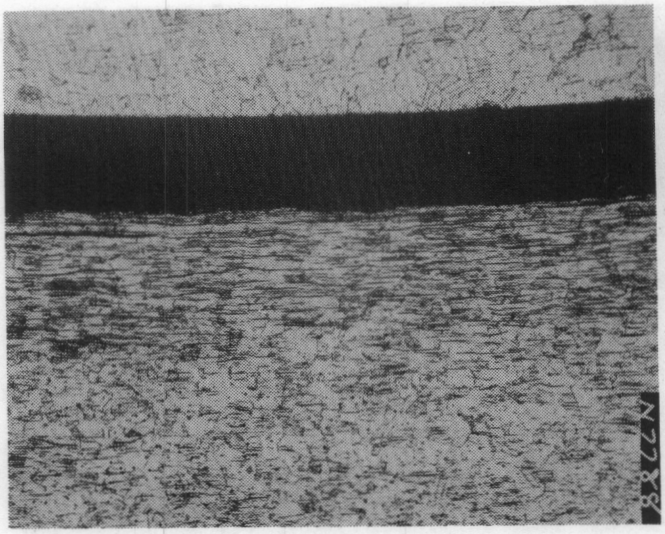

a. At 50X

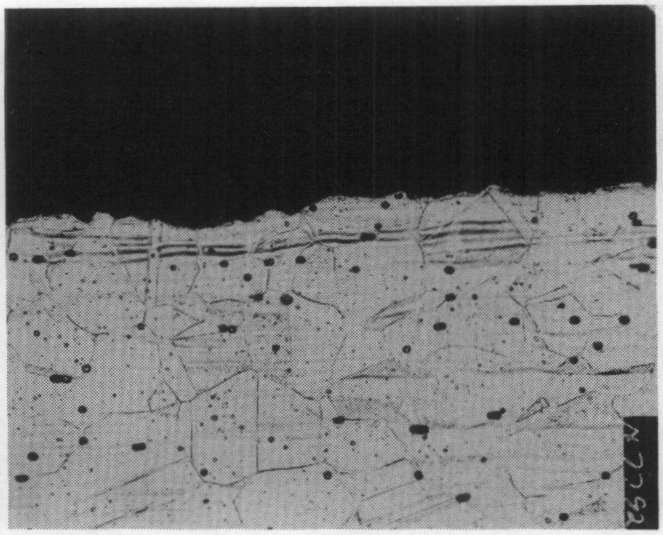

b. At 225X

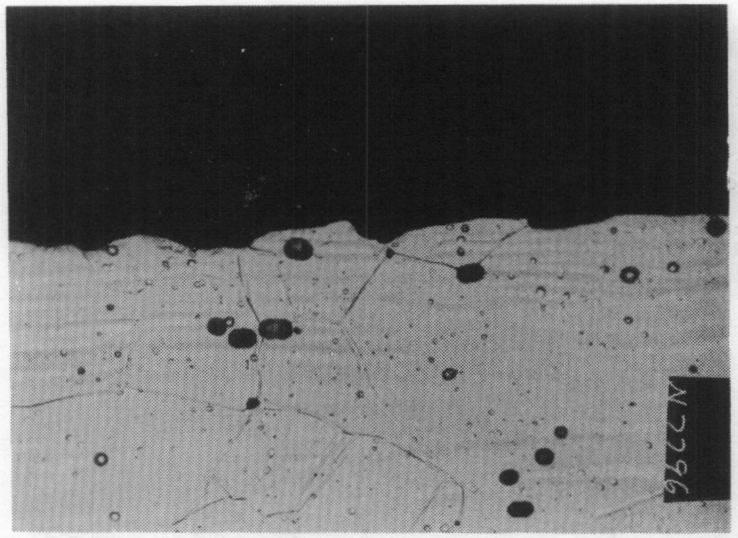

c. At 500X

Figure 30. Photomicrographs of Capsule C-73, Ring 3, Etched

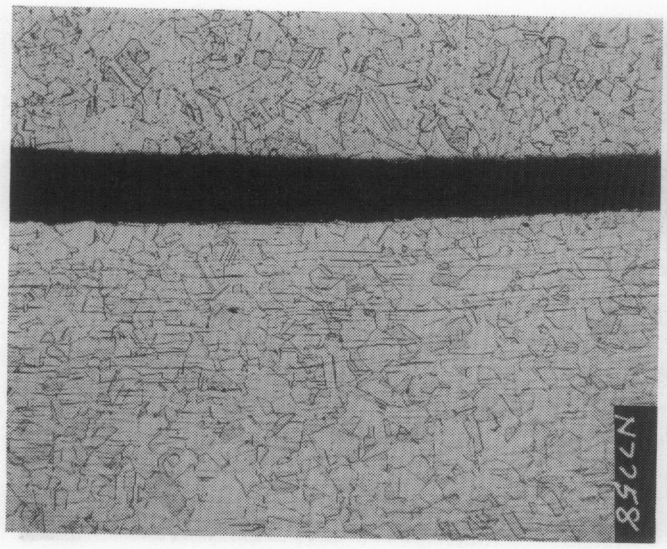

a. At 50X

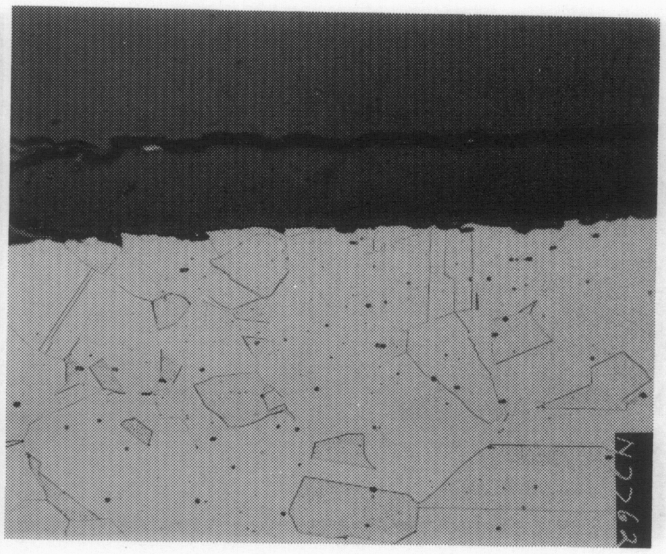

b. At 225X

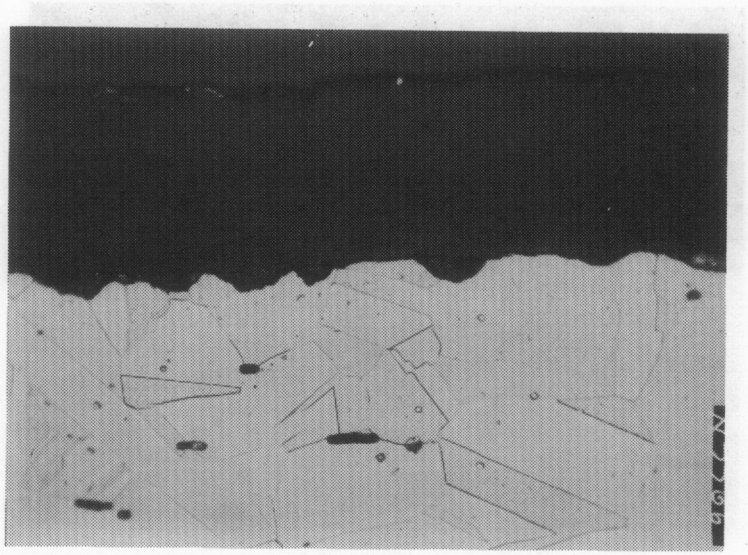

c. At 500X

Figure 31. Photomicrographs of Capsule C-74, Ring 2, Etched

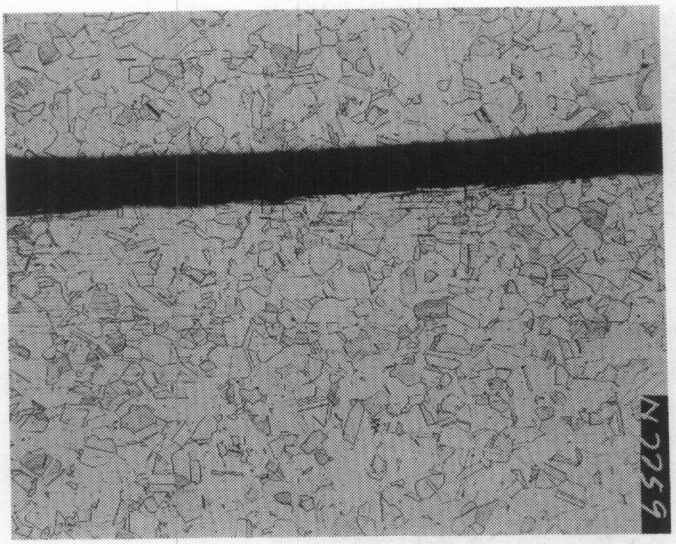

a. At 50X

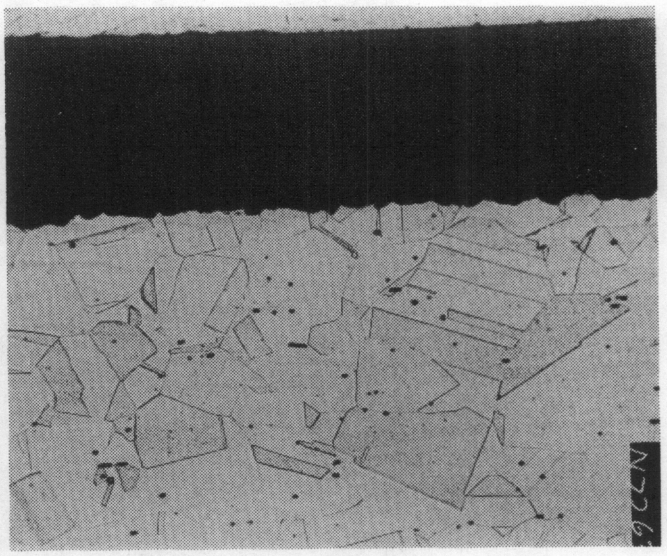

b. At 225X

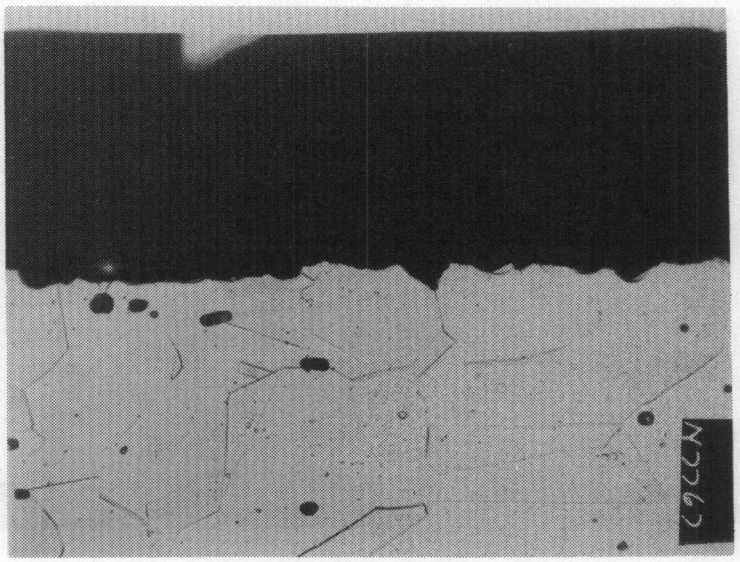

c. At 500X

Figure 32. Photomicrographs of Capsule C-74, Ring 3, Etched

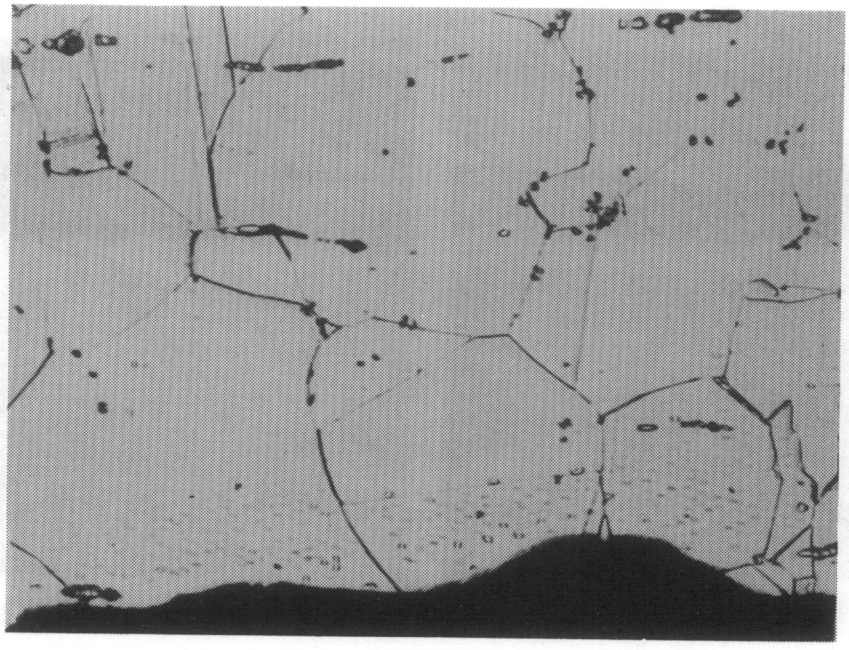

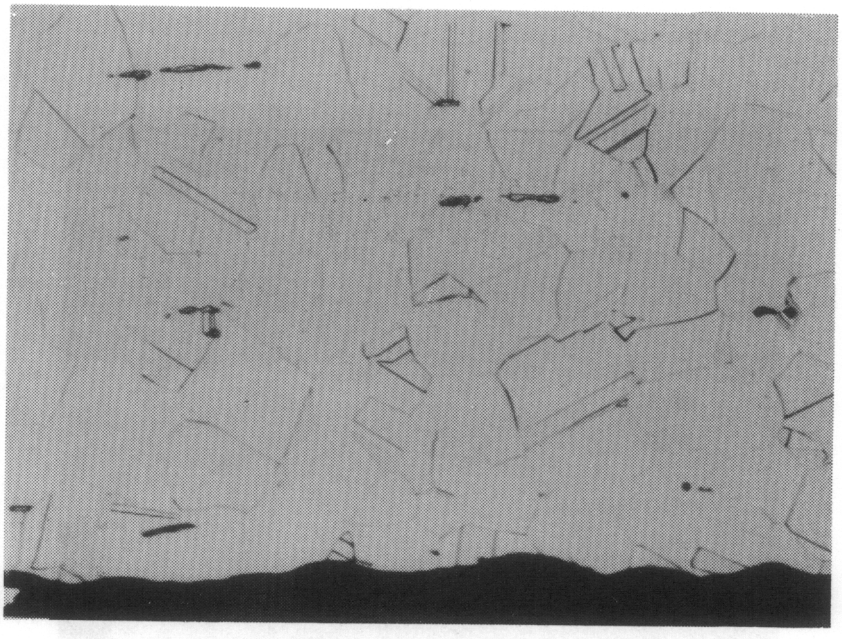

Figure 33. Photomicrographs of Zero-Time Capsule, Etched, 500X

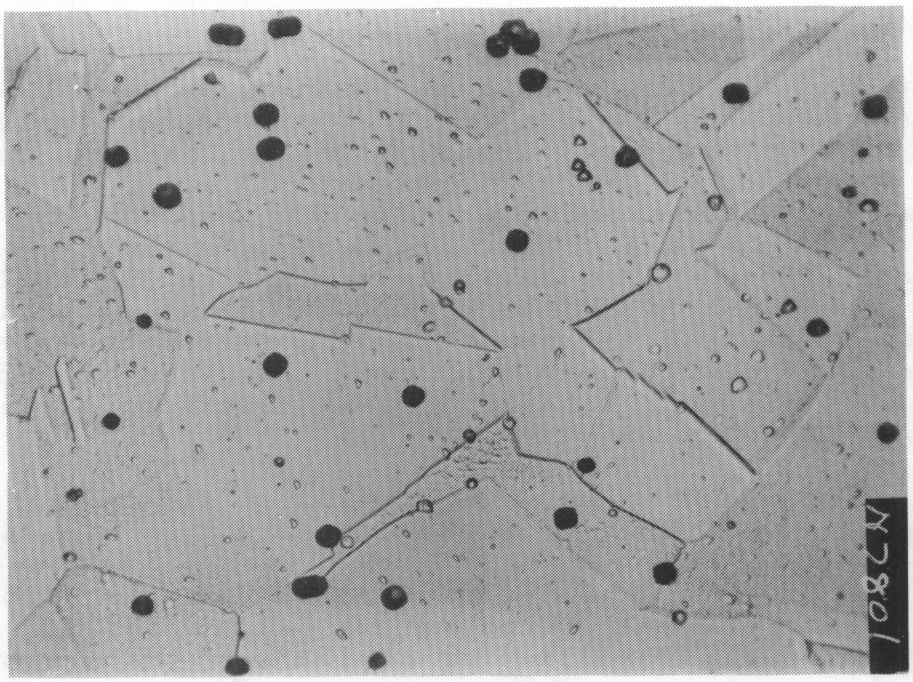

Figure 34. Photomicrograph of Capsule C-73, Etched Section Center, 500X

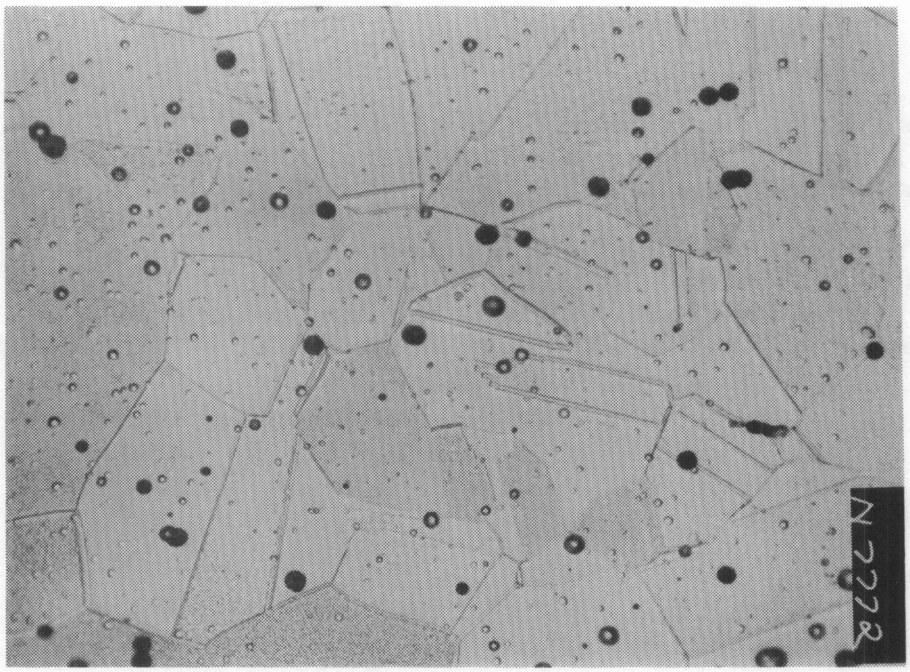

Figure 35. Photomicrograph of Capsule C-74, Etched Section Center, 500X

The micrographs were used to estimate the corrosion and overall wall thicknesses. Estimates of metal attack were based on measurements of the maximum surface irregularity as found in the 225X photomicrographs (Table 7). As compared with the zero-time capsule metal attack, the approximate 0.001-in metal attack measured in capsules C-73 and C-74 is well within the estimated metal attack resulting from melt casting (Bryan, 1984). Thus there appears to have been no measurable amount of metal loss in these capsules during the 5 years of use in the SIDSS irradiator.

In addition, each ring section was measured for overall capsule wall thickness using the 36.5X photomicrographs. The thickness measurements that were determined mechanically and the thickness measurements that were made using the photomicrographs are listed in Table 8. There is good correlation (within 0.001 in) between the measurement methods. All of these capsule wall measurements fall well within the wall thickness specifications for the original capsule material.

Corrosion rates at normal irradiator temperatures (inner wall temperature = 150° to 250°C) are too low to measure. We have, therefore, used corrosion rate data in the temperature range of 392° to 454°C to evaluate potential corrosion on capsules in deep geologic disposal (Bryan, 1985) and a single measurement made at 800°C during a high temperature test using nonradioactive salt in a WESF container (Tingey et al., 1985). When these data are plotted on an Arrhenius plot (log rate versus 1/T), shown in Figure 36, the straight line through the plots yields the following rate expression:

$$\text{rate} = 4.8 \times 10^{10} \quad e^{-40,600/RT} \ \mu m/h.$$

These data extrapolate to a rate of 8×10^{-9} μm/h (9×10^{-8} in/30 yr), 1.6×10^{-5} μm/h (0.0002 in/30 yr) and 2.7×10^{-4} μm/h (0.003 in/30 yr) at 200°, 300°, and 350°C, respectively. These data are consistent with the lack of an observable corrosion rate on the samples from the SIDSS capsule operating at interface temperatures of about 200°C. Recognizing the limited amount of corrosion data available to develop the rate equation, it nevertheless appears that a salt-stainless steel interface temperature of 350°C would not yield unacceptable corrosion rates.

Table 7

Estimates of Metal Attack

	Depth of Attack (in)			
Capsule	Ring 1[a]	Ring 2	Ring 3	Ring 4
C-73	0.0009	0.0007	0.001	0.0005
C-74	0.0006	0.0004	0.0005	0.0006

[a]See Figure 2 for ring location on capsule.

Table 8

Metallography Section Thickness Measurements on Capsules C-73 and C-74[a]

	Thickness (in)							
Measurement	Capsule C-73				Capsule C-74			
Technique	Ring 1	Ring 2	Ring 3	Ring 4	Ring 1	Ring 2	Ring 3	Ring 4
Mechanical	0.094	0.094	0.094	0.091	0.094	0.096	0.094	0.095
Photomicro-graphic	0.095	0.095	0.094	0.092	0.093	0.096	0.093	0.096

[a]See Figure 2 for ring location on capsule.

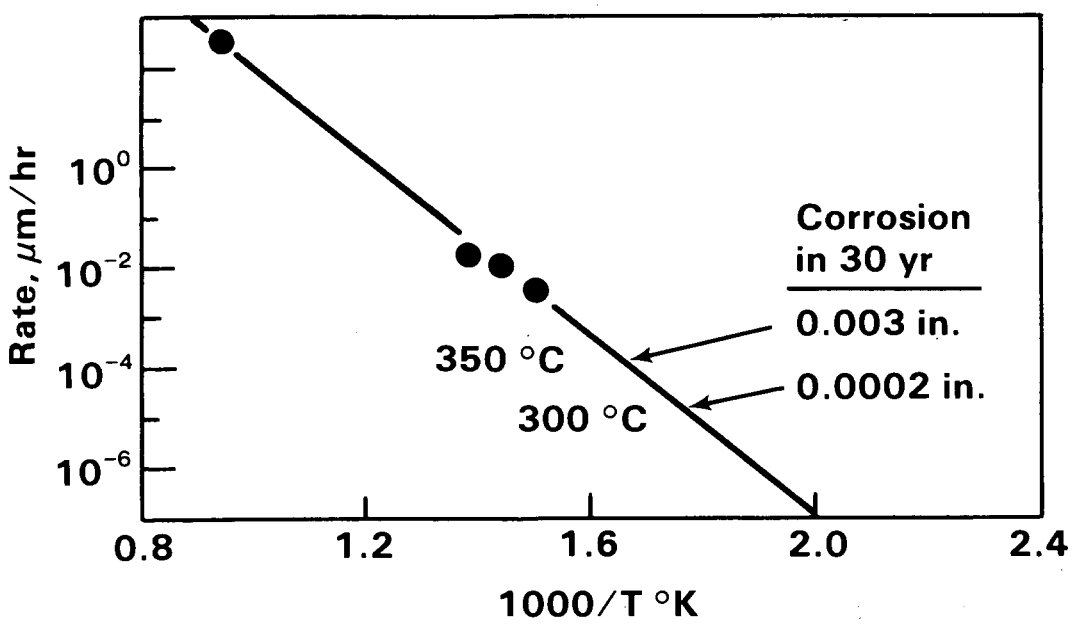

Figure 36. Corrosion Rate of WESF Cesium Capsules

7. MICROPROBE ANALYSIS

One set of capsule wall samples was selected for microprobe analysis. Since no significant differences were found between the two capsules in the optical examination, capsule C-73 was arbitrarily selected. The purpose of the microprobe analysis was to compare the composition of the capsule wall at the salt/metal interface with the bulk composition. In addition, the grain boundaries were checked for the presence of impurities that could be associated with the CsCl salt.

Samples from rings 1, 2, 3, and 4 were examined. Areas of primary interest for this examination were the grain boundary intersections of the salt/metal interface where a notch or depression was located. Both energy-dispersive spectrometry (EDS) and wavelength-dispersive spectrometry (WDS) data were acquired, producing the same results. No cesium, chlorine, or any other element that would not be found in the Type 316 SS was detected.

A profile of the iron, chromium, and nickel concentrations was made from the salt/metal interface to a distance 160 μm from the salt/metal interface; data were collected at 2-μm intervals. These data showed no systematic change in composition between the sample interior and the interface area. Within the limits of the microprobe, there was no elemental diffusion within the stainless steel, and there was no evidence of grain boundary attack by the cesium chloride or any impurity in the salt.

8. ISOTOPIC AND CHEMICAL ANALYSIS OF THE SALT

The behavior of the salt in the capsule depends largely on the purity. The corrosion rate of the salt with the stainless steel container is controlled mainly by the content of reactive impurities (Fullam, 1982). Furthermore, the melting point is reduced markedly by impurities. Therefore, it was important to attempt to analyze the salt to determine the composition. Earlier efforts to determine the composition of the salt yielded inconsistent and inconclusive results (Tingey, Wheelwright, and Lytle, 1984). In order to obtain more information on the composition of the salt, samples were removed from the capsules following cutting of the capsule container. These samples were placed in small bullets made from 3/8-in tubing with Swagelok* caps on each end. As indicated in Section 4, six of the eight salt samples had at least one of the end caps off when the bullets were received. The other two bullets had less sample than desired and were contaminated with visible metal chips. These effects combined to limit the number of analyses. To supplement the data obtained from capsules C-73 and C-74, analyses of salt samples from five other capsules, which were opened to supply Cs-137 to fabricate waste glass for canister studies, are included in this report.

Samples were prepared for analysis by weighing the dried samples and dissolving them in a 2 percent nitric acid (HNO_3) solution. Only about 0.1 g of salt was available for dissolution. Of this amount, 7 and 12 percent were insoluble from capsules C-73 and C-74, respectively. The residue was then dried and weighed and an attempt was made to dissolve it in concentrated HNO_3. Under this treatment, about 75 percent of the residue dissolved, and analysis showed that the portion of the residue soluble in concentrated HNO_3 was primarily Fe, Cr, and Ni. This analysis led us to conclude that the portion of the residue soluble in concentrated HNO_3 was small stainless steel chips from the cutting of the capsule. The remaining insoluble portion (~25 percent) was assumed to have come from the salt sample and is believed to be the resin used in the recovery and purification of the cesium.

The portion of the salt soluble in the 2 percent HNO_3 was analyzed by inductively coupled plasma (ICP) atomic emission spectroscopy to determine the cationic impurities, gamma scanning to determine the Cs-137 content, and mass spectroscopy to determine the isotopic ratio of the various cesium isotopes. The ICP analyses were performed on an Applied Research Laboratories ARL-34000 atomic emission spectrometer modified to allow analysis of high-level radioactive solutions. The sample sizes were minimized to limit personnel exposure by the highly radioactive

---

*Swagelok Tube Fittings, Crawford Fitting Co., 29500 Solon, Solon, Ohio.

Cs-137. This sample preparation resulted in a high-dilution factor (~1000:1). For these diluted samples, a realistic detection limit is approximately 0.05 wt% for most of the impurity cations. The results of the elemental analyses are shown in Table 9 for the five additional capsules as well as the two capsules removed from SIDSS. Although there is some variability in the results from sample to sample, the results are as consistent as can be expected for the wide variety of capsules chosen. These differences can be due to batch-to-batch differences, time of decay, and perhaps contamination during the capsule opening and sampling procedure. The sample from Capsule C-366 had an unusually high content of Fe, Cr, and Ni and also contained several elements not found in the other capsules. It appears that this salt was contaminated with stainless steel either during processing or during capsule cut up. Sample C-73 had unusually high Na content and sample C-74 showed a significant amount of K, which was only detected in one other capsule. The main impurity in all capsules was barium, most of which was generated during the decay of the Cs-137 to Ba-137.

The ICP analyses include only the cations; anionic species were assumed to be the chloride except for boron, which does not form a stable solid chloride. Thus, we used the boron oxide (B_2O_3) compound in these calculations. The percentages of the impurity compounds are shown in Table 10 for the seven capsules. The total of the soluble impurities range from 5.3 to 19.6 percent. This wide spread is largely due to the high concentration of Fe, Cr, and Ni in capsules C-366 and C-73. The range of variance in the other capsules is not unexpected. These analyses appear to be considerably more consistent than those reviewed by Tingey, Wheelwright, and Lytle (1984) and thus are considered more representative of the WESF capsules composition.

An aliquot of the diluted solution was taken for gamma counting and isotopic analysis. The gamma counting was performed using a germanium-lithium detector with a Tracor Northern TN-4000 analyzer. The isotopic analyses used a Consolidated Electrodynamics Corporation CEC-703 mass spectrometer modified to handle radioactive samples.

The specific activity of the samples was calculated and is shown in Table 11. Also listed in the table is the activity determined by calorimetry of the capsules, decayed to correspond to the time of the gamma count. On the average, the gamma count activity was 4 percent lower than the activity determined by calorimetry with a range from 7 percent higher (C-74) to 18 percent lower (C-134). Also listed in Table 11 are the results of the isotopic analyses for the detectable cesium isotopes. The gamma count was used to calculate the Cs-137 content. This was then used to calculate the total cesium in the sample and the total fraction of the sample, which was CsCl. The sum of the CsCl and the total impurity fraction taken from Table 10 shows the mass balance for the soluble portion of the salt.

Table 9

Elemental Analysis of Impurities (Wt%)

	Capsule Number						
Impurity	C-74	C-73	C-206	C-134	C-17	C-130	C-366
Ba	6.0	6.5	4.8	5.1	4.3	3.1	3.2
Ba [decay][a]	[5.3]	[4.6]	[3.9]	[4.2]	[4.3]	[4.9]	[2.0]
Ca	0.03	0.06	0.02	0.02	0.02	0.01	0.19
Cr	0.1	0.3	0.2	0.05	0.1	0.02	0.5
Fe	0.2	0.8	0.2	0.2	0.1	0.04	1.6
Mg	b	b	0.005	0.01	0.003	b	0.05
Mn	b	0.04	0.01	0.02	0.006	0.005	0.09
Na	0.04	1.5	0.7	0.1	0.3	0.1	0.3
Ti	b	b	0.03	0.02	0.04	0.02	0.03
Zr	b	b	0.04	0.02	0.04	0.01	0.04
Ni	0.06	0.1	0.02	0.06	b	0.02	1.5
B	0.04	b	b	0.01	0.03	b	0.02
Mo	0.06	0.26	b	b	0.06	b	0.05
Al	0.1	b	b	b	b	b	0.1
Ce	b	b	b	b	b	b	0.01
K	0.7	b	b	b	b	b	0.7
La	b	b	b	b	b	b	0.01
Si	b	b	b	b	b	b	0.2
Sr	b	b	b	b	b	b	0.005
Total	7.3	9.6	6.0	5.6	5.0	3.3	8.6

[a]Not included in total.
[b]Analyzed elements that were nondetectable.

Table 10

Impurity Content from Elemental Analysis (Wt%)

Impurity Compound	Capsule Number						
	C-74	C-73	C-206	C-134	C-17	C-130	C-366
$BaCl_2$	9.1	9.9	7.3	7.8	6.5	4.7	4.9
$CaCl_2$	0.08	0.17	0.06	0.06	0.06	0.03	0.53
$CrCl_3$	0.3	0.9	0.6	0.2	0.3	0.1	1.5
$FeCl_3$	0.6	2.3	0.6	0.6	0.3	0.1	4.7
$MgCl_2$	a	a	0.02	0.04	0.01	a	0.2
$MnCl_4$	a	0.14	0.04	0.07	0.02	0.02	0.32
NaCl	0.01	3.8	1.8	0.3	0.8	0.3	0.8
$TiCl_4$	a	a	0.1	0.1	0.2	0.08	0.1
$ZrCl_2$	a	a	0.07	0.04	0.07	0.02	0.07
$NiCl_2$	0.13	0.22	0.04	0.13	a	0.04	3.32
B_2O_3	0.13	a	a	0.03	0.10	a	0.06
$MoCl_3$	0.13	0.55	a	a	0.13	a	0.11
$AlCl_3$	0.5	a	a	a	a	a	0.5
$CeCl_3$	a	a	a	a	a	a	0.02
KCl	1.3	a	a	a	a	a	1.3
$LaCl_3$	a	a	a	a	a	a	0.02
$SiCl_4$	a	a	a	a	a	a	1.2
$SrCl_2$	a	a	a	a	a	a	0.01
Total	12.4	18.0	10.6	9.2	8.4	5.3	19.6

[a]Analyzed elements that were nondetectable.

Table 11

Activity and Isotopic Analysis

		Capsule Number						
Measurement	Units	C-74	C-73	C-206	C-134	C-17	C-130	C-366
Gamma count	Ci/g[a]	21.1	19.2	18.2	17.5	16.0	20.3	15.5
Calorimetry	Ci/g[a]	19.7	19.5	19.7	20.7	16.7	20.7	15.5
Cs-133	Atom %	55.3	55.3	55.0	54.5	61.7	54.6	55.0
Cs-134	Atom %	0.0	0.0	0.0	0.0	0.0	0.0	0.0
Cs-135	Atom %	12.8	12.8	13.0	13.2	11.1	13.2	14.0
Cs-137	Atom %	31.9	31.9	32.0	32.4	27.2	32.2	31.0
CsCl content	%	95	87	82	77	85	91	72
Impurity content	%	12.4	18.0	10.6	9.2	8.4	5.3	19.6
Mass balance	%	107	105	93	86	93	96	92

[a]Weight of material dissolved in 2 percent HNO_3

The mass balance, also given in Table 11, indicates that the analyses are reasonably representative of the capsule contents. In our opinion, these analyses yield useful data and markedly increase our understanding of the capsule content. They clearly show the variability of the salt in the capsules analyzed, but also indicate the probable range of salt compositions. At these low temperatures, no correlation can be made between capsule inner wall corrosion and salt composition because the corrosion rate is so low. However, at higher temperatures, one might expect to see such a correlation.

9. CONCLUSION

Two WESF capsules containing CsCl from the SIDSS irradiator were destructively tested after 60 months of service in a dry irradiator environment. Metallographic samples were taken to study the corrosion resistance of the capsule material. Samples of the CsCl salt were taken for chemical impurity, radiochemical, and isotopic analysis. Four methods were used to examine the capsule wall material: visual surface inspection, mechanical thickness measurement, optical microscopy, and microprobe elemental analysis. Although each method was independent, there was usually a correlation among the results. The salt samples were taken to obtain data on the impurity level in the salt and activity levels of the CsCl. The chemical analysis by ICP provided a measurement of the level of impurities and elemental type. The radiochemistry and isotopic analyses provided data for specific activity calculations, which were used as a method to confirm the calorimetry measurements.

The visual surface examination revealed no distinct signs of pitting, although the surfaces were discolored. The appearance of the rings ranges from bright to dark, with ring 4 being the brightest.

The mechanical thickness measurements revealed no significant wall thickness variations. The capsule C-73 wall was 0.093 ±0.003 inches thick; capsule C-74, 0.095 ±0.003 inches thick. The specification for the material was 0.095 ±0.009 inches. Both capsules were well within the specification. The wall thickness measurements of the metallography section verified the mechanical measurements.

An examination of the etched microstructure revealed no significant differences between any of the rings, and there was no microstructural indication of a measurable attack. The irregularities that were observed are comparable to those found on the zero-time capsule (Bryan, 1985), which indicated an initial metal loss of approximately 0.001 inches when the molten salt was poured into the capsule. The optical examination of the welds (top and bottom) revealed good weld penetration and no signs of corrosion. Microprobe elemental analysis of capsule wall samples indicated that no significant diffusion occurred at the ID surface and no impurities attacked the grain boundaries.

From these studies, we conclude that the corrosion rate is so small at the temperature experienced in SIDSS that corrosion cannot be observed after five years at temperature.

The radiochemistry and isotopic analyses provided a ratio of the cesium isotopes and gamma count to measure the Cs-137 isotope. The activity that was calculated from these data provide a

irect comparison to the measured calorimetry of the capsule before sectioning. These analyses showed good correlation with the calorimetry. The chemical impurity analysis by ICP indicated that the bulk of the soluble impurity was Ba. Since Ba is a decay product of Cs-137, the level of Ba will continue to increase with time. When the decay product Ba* is subtracted from the total Ba, the impurity level is between 1 and 6.5 elemental wt%. The concentration of the individual elements that were detected fall within previous estimates from analytical determination of the WESF process.

The results of these analyses indicate that the predicted impurity levels in the salt are reasonable and that the measured calorimetry of the SIDSS capsules is within the estimated range of error of that measurement.

---

*As determined from the date the sale was encapsulated.

10. REFERENCES

Bryan, G. H., 1985, Cesium Chloride Compatibility Testing Program Annual Report Fiscal Year 1984, Pacific Northwest Laboratory, Richland, Washington, PNL-5341.

Fullam, H. T., 1982, Cesium Chloride Compatibility Testing Program Annual Report Fiscal Year 1982, Pacific Northwest Laboratory, Richland, Washington, PNL-4556.

Kenna, B. T., 1982, WESF ^{137}Cs Gamma Ray Sources, Sandia National Laboratories, Albuquerque, New Mexico, SAND82-1492.

Kenna, B. T. and F. J. Schultz (ORNL), 1983, Characterization of Aged WESF Capsules, Sandia National Laboratories, Albuquerque, New Mexico, SAND83-0928.

Tingey, G. L., E. J. Wheelwright, and J. M. Lytle, 1984, A Review of Safety Issues That Pertain to the Use of WESF Cesium Chloride Capsules in an Irradiator, Pacific Northwest Laboratory, Richland, Washington, PNL-5170.

Tingey, G. L., et al., 1985, WESF Cesium Capsule Behavior at High Temperature or During Thermal Cycling, Pacific Northwest Laboratory, Richland, Washington, PNL-5517.

APPENDIX A

TEMPERATURE MODEL BASED ON SIDSS IRRADIATOR CAPSULE CONFIGURATION

JACK TILLS

In March of 1983, temperature measurements were made on four WESF cesium chloride capsules and the source plaque with the source in the operating position (Figure A.1) There was no air flow across the plaque; the blowers had been turned off 24 h prior to the start of the measurements. The temperature measurements were made with an array of five thermocouples woven into the asbestos cloth pads of the remotely operated "swipe" apparatus, initially designed to obtain "swipe" samples of the capsule surfaces. Contact between the thermocouples and the capsule surface was of a sliding nature, thus (1) the absolute temperatures as measured are probably biased to the low side and (2) there was a maximum spread of 10°C between the highest and lowest thermocouple readings at any given point on the surface of the capsule.

The temperature measurements of the capsules mounted horizontally in the source plaque indicate that the difference between the tops and bottoms of the capsules were approximately 60°C. The temperature of the plaque structure, or source holder, was 12°C. The circumferential temperature difference was attributed to the variation of the inner to outer wall gap while the capsule was in the horizontal position. The configuration extremes between the inner and outer capsules for the WESF capsule are shown in Figure A.2.

The purpose of the heat transfer analysis was to determine eccentricity effects on the WESF (salt-inner capsule wall) maximum temperatures. Experimental results (temperature measurements) from SIDSS were used to define outer boundary temperatures for the calculations, which were run using the TAC2D heat transfer code.* An R-theta model was used, allowing theta dependence for the inner to outer wall gap and outer boundary temperature. Three calculations were run to study eccentricity effects for a capsule having a 150 watt uniform** heat source. The calculations were:

1. Symmetric gap, T_{outer} (θ) = 373 K

2. Asymmetric gap (horizontal position), T_{outer} (θ) = 373 K

---

*J. F. Peterson, TAC2D, A General Purpose Two-Dimensional Heat Transfer Computer Code, Phillips General Atomic, San Diego, CA, GA-8868 (UC-32) September 1969.

**Attachment 1 to this appendix.

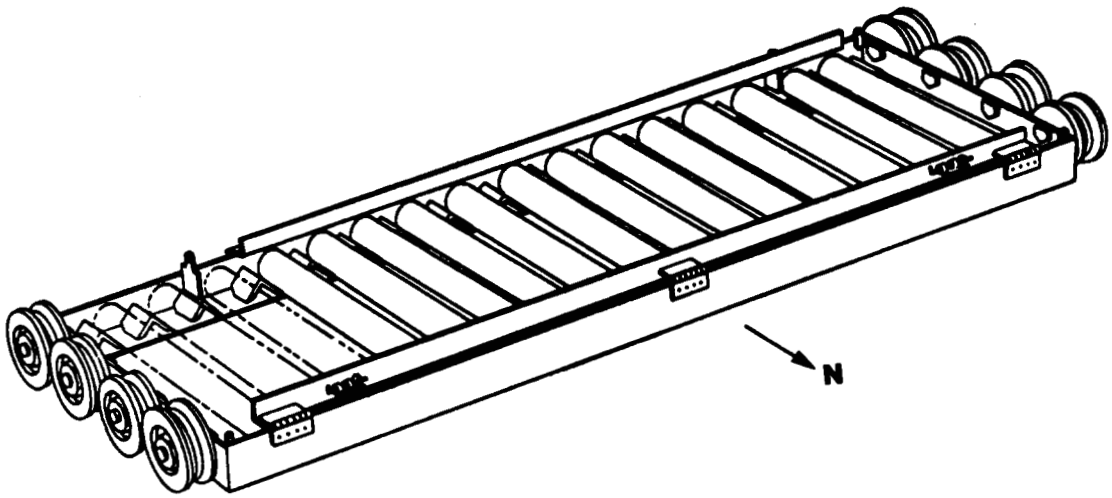

Figure A.1. Gamma Source Plaque

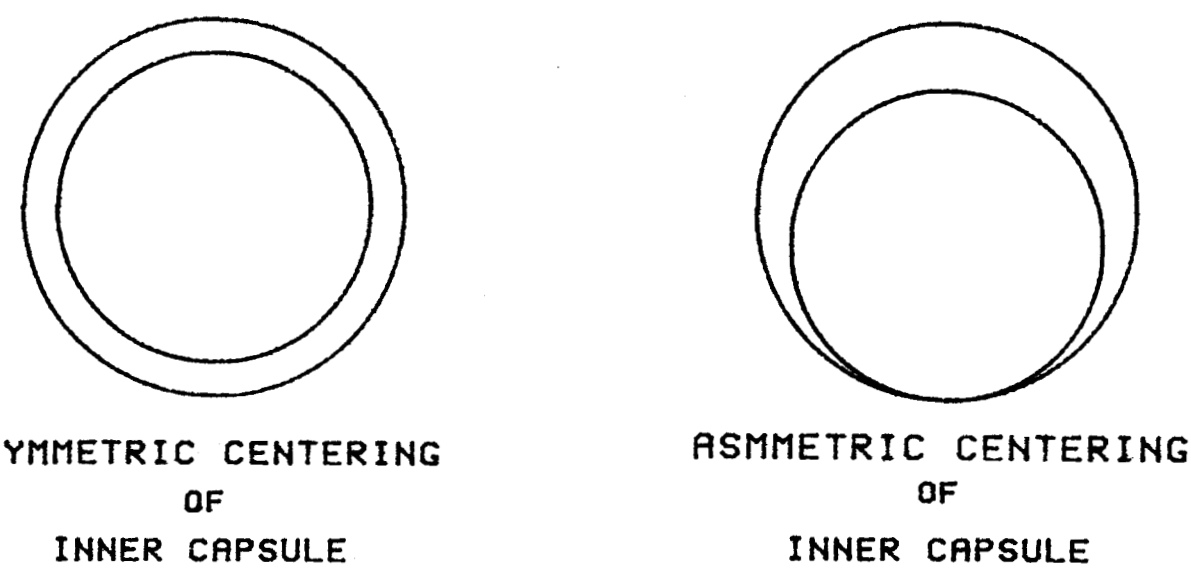

Figure A.2. WESF Capsule Geometries for R-θ Heat Transfer

3. Asymmetric gap, T_{outer} (θ) = max-min variation with θ

The T_{outer} (θ) variation for the last case was taken to be the max-min experimentally determined ΔT with linear theta dependence. The finite difference mesh is shown in Figure A.3 and temperature maps for each calculation are given in Figures A.4 through A.6. From these results it can be concluded that the asymmetric configuration gives lower maximum temperatures than the symmetric calculations for equal outer-wall temperature. Variations in outer-wall temperatures will not change this conclusion, however, more complete and detailed experiments on WESF capsules may be needed to verify temperature variations observed.

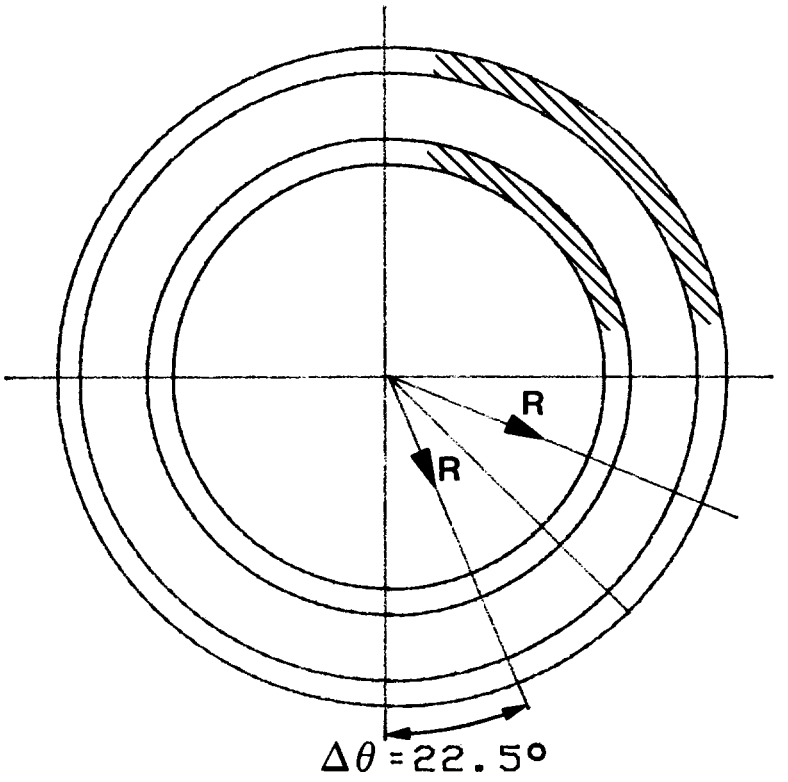

Figure A.3. Finite Element Mesh

TOP

CsCl

Inner Wall

Outer Surface

θ (K)	0.131	0.392	0.654	0.916	1.177	1.439	1.701	1.962	2.224	2.486	2.677	2.797	Surface
168.75													
146.25													
123.75													
101.25	547	546	544	540	535	530	523	515	506	495	489	489	373
78.75													
56.25													
33.75													
11.25													

R (cm)

BOTTOM

Figure A.4. Symmetry Configuration Temperature MAP (K) as a Function of θ & R

TOP

CsCl

Inner Wall

Outer Surface

θ(K)	0.131	0.392	0.654	0.916	1.177	1.439	1.701	1.962	2.224	2.486	2.677	2.797	Surface
168.75	486	487	488	487	485	481	477	471	464	456	451	451	373
146.25	486	487	487	485	483	479	475	469	462	453	448	448	373
123.75	485	486	485	483	480	476	471	464	457	448	443	443	373
101.25	485	484	483	480	476	471	465	458	450	441	436	436	373
78.75	484	482	480	476	471	465	458	451	441	431	426	425	373
56.25	484	481	477	472	466	459	451	442	432	420	414	414	373
33.75	483	480	475	469	462	453	444	433	421	408	400	400	373
11.25	483	479	474	467	459	450	440	429	416	402	395	394	373

R (cm)

BOTTOM

Figure A.5. Asymmetric Configuration Temperature MAP (K) as a Function of θ & R

TOP

CsCl

Inner Wall

Outer Surface

θ (K)	0.131	0.392	0.654	0.916	1.177	1.439	1.701	1.962	2.224	2.486	2.677	2.797	Surface
168.75	489	490	490	489	486	482	477	471	464	455	450	450	340
146.25	489	490	489	488	485	481	476	469	462	453	448	448	340
123.75	489	489	488	486	482	478	472	466	458	449	444	444	355
101.25	488	488	486	483	479	474	468	461	452	443	438	437	355
78.75	488	486	484	480	475	469	462	454	445	435	429	429	370
56.25	487	485	481	477	471	464	456	447	437	426	420	420	370
33.75	487	484	479	474	467	459	450	440	429	416	409	408	385
11.25	487	483	478	472	465	457	447	437	425	412	404	404	385

R (cm)

BOTTOM

Figure A.6. Asymmetric Configuration Temperature MAP (K) as a Function of θ & R

Attachment 1

ENERGY DISTRIBUTION FOR THE WESF CAPSULE

DON McKEON

INTRODUCTION

The purpose of this report is to estimate the energy deposition rate in a WESF CsCl source capsule by calculating the amount of radiation that is deposited in the source capsule. In order to determine the energy deposition rate in a WESF capsule, it is first necessary to study the nuclear decay chain of cesium-137 to determine the types and quantities of radiation emitted from a capsule. Once this has been completed, Monte Carlo radiation transport codes will be used to determine the amount of the radiation that has been deposited as heat in the WESF source capsule. In addition, the amount of energy that escapes from the capsule, but is later deposited as heat in a large storage pool, will also be determined.

This report is divided into six sections. The first section of this report summarizes several key concepts of radioactive decay (some readers may wish to skip this section). Section II discusses the radioactive decay of cesium-137. Section III presents the WESF source capsule. Section IV discusses the radiation transport calculations used to estimate the energy deposition rate in the WESF source capsules. Section V discusses the derivation of the equations describing the heat generation rates for WESF capsules. Section VI is a brief summary of the energy deposition calculations.

I. SUMMARY OF RADIOACTIVE DECAY

A brief review of some of the more important concepts of nuclear physics and radioactive decay will be discussed here. The reader is encouraged to make use of References 1, 2, 3, 4, and 5 to further their knowledge about this topic beyond this simplistic discussion.

I.A Radioactive Decay

The probability per unit time that a radioactive isotope will decay is a constant and independent of time. This constant is called the decay constant and is denoted by λ. The rate of change of the undecayed nuclei can be denoted by

$$\frac{dN}{dt} = -\lambda N(t) \quad , \tag{1}$$

where N(t) represents the isotope's concentration as a function of time. Solving for N(t), with some initial concentration $N(0) = N_o$, the concentration of nuclei at time t is given by

$$N(t) = N_o e^{-\lambda t} \quad . \tag{2}$$

The activity of this isotope, denoted by R(t), is given by multiplying the decay constant by the concentration, or

$$R(t) = \lambda N(t) \quad . \tag{3}$$

The half-life of a radioactive isotope, denoted by $\tau_{1/2}$, is the time required for the concentration of the isotope to be reduced by one half. By setting the left side of Equation (2) to $0.5N_o$ and solving for $t = \tau_{1/2}$, the half-life can be shown to be equal to

$$\tau_{1/2} = \frac{\ln 2}{\lambda} \quad . \tag{4}$$

I.B Secular Equilibrium

The previous discussion dealt only with the decay of an isotope that was not being produced as a function of time. If a decay chain is represented by

$$A \longrightarrow B \longrightarrow C,$$

then the concentration of isotope B (or C) cannot be determined from Equation (2). Rather, the equation for the concentration of isotope B as a function of time is given by: [4]

$$N_B(t) = N_{Bo}e^{-\lambda_B t} + \frac{N_{Ao}\lambda_A}{\lambda_B - \lambda_A}\left(e^{-\lambda_A t} - e^{-\lambda_B t}\right) . \qquad (5)$$

If the isotope A decays much more slowly than isotope B, that is, if $\lambda_A << \lambda_B$, and neglecting the initial concentration of B, then the concentration of isotope B can be expressed as

$$N_B(t) = \frac{\lambda_A}{\lambda_B} N_{Ao}\left(1 - e^{-\lambda_B t}\right) . \qquad (6)$$

After some delay, the decay rate of the daughter isotope B will equal the decay rate of the parent isotope A. This is, when $\lambda_B t >> 0$, then the decay rates of A and B are given by

$$R_A(t) = \lambda_A N_{Ao}(t) \cong \lambda_B N_B = R_B(t) . \qquad (7)$$

This is called secular equilibrium.

I.C Beta-Minus Decay

Beta-minus decay is the transformation of one neutron in the nucleus to a proton, electron or beta-ray (β^-), and antineutrino ($\bar{\nu}$). The beta-decay process can be represented as

$$^{A}_{Z}X \longrightarrow ^{A}_{Z+1}Y + \beta^- + \bar{\nu} . \qquad (8)$$

The energy released in beta-decay, called the Q-value of the decay process, is shared by the recoil nucleus, the emitted electron, and the antineutrino. The energy of the recoil nucleus is of little interest because of its low energy, usually below the atom's ionization energy. The remaining energy released in the decay process is shared between the electron and the antineutrino. The electrons are emitted with a continuous energy

spectrum ranging from zero to the "beta endpoint energy", denoted by E_{max}, which is equal to the Q-value of the beta-minus decay. For beta-minus decay, the average electron energy is about 0.3 times E_{max}.[4] The antineutrino is also emitted with a continuous energy spectrum ranging from zero to E_{max} with an average energy of about $0.7E_{max}$. Since the antineutrino is neutrally charged and has a very low probability of interacting with matter, the antineutrino energy is not recoverable.

In summary, beta-minus decay occurs when a neutron in a nucleus decays to a proton, electron, and antineutrino. The electron and antineutrino share the energy of the decay process, which is called the Q-value for the reaction. The electron energy varies between zero and the beta endpoint energy, E_{max}, with an average energy of about $0.3E_{max}$. The average energy of the antineutrino is about $0.7E_{max}$. Due to the extremely low probability of an antineutrino interacting with matter, the antineutrino energy cannot be recovered.

I.D Gamma Decay and Internal Conversion

A nucleus in an excited state can decay to lower-lying levels or to the ground state by one of two competing modes: gamma-ray emission or internal conversion. In gamma-ray emission, the nucleus decays to a lower-lying level by emitting a gamma-ray photon with an energy equal to the differences between the initial and final energy levels, i.e., the decay energy. Competing with gamma-ray emission is internal conversion. In internal conversion, the excited nucleus decays to a lower-lying level by ejecting an orbital electron from the atom with an energy equal to the decay energy minus the electron binding energy. The electron binding energy is then emitted either as X-rays or as Auger electrons.

II. REVIEW OF THE DECAY CHAIN OF CESIUM-137

The data listed in this section is taken from the Table of Isotopes by C. M. Lederer et al.[6].

II.A Cesium-137 Decay to Barium-137

^{137}Cs beta-minus decays to ^{137}Ba with a half life of 30.174 years by one of two transitions. The high-energy beta transition to the stable ground state of ^{137}Ba occurs in 5.4 percent of the ^{137}Cs decays. The Q-value for the high-energy transition is 1.173 MeV. The low-energy beta transition to the metastable state of ^{137}Ba (^{137m}Ba) occurs in 94.6 percent of the ^{137}Cs decays. The Q-value for the low-energy transition is 0.51163 MeV. The metastable state of ^{137}Ba decays with a half-life of 2.5513 minutes to the ground state of ^{137}Ba either by gamma-ray emission or internal conversion. Gamma-ray emission occurs in 89.9 percent of the transitions and internal conversion occurs in

the remaining 10.1 percent. The energy of the ^{137m}Ba gamma-ray is 0.66165 MeV. This gamma-ray is often called the ^{137}Cs gamma-ray since it occurs at a rate proportional to the decay rate of ^{137}Cs (i.e., ^{137}Cs and ^{137m}Ba are in secular equilibrium). A summary of the ^{137}Cs decay chain data is listed in Table A1.1. The decay scheme for ^{137}Cs is illustrated in Figure A1.1.

III. WESF SOURCE CAPSULE

The stainless steel encapsulated WESF cesium-chloride capsule is illustrated in Figure A1.2. The outside dimensions of the capsule are 52.8 cm (length) by 6.7 cm (diameter) (20.775 x 2.625 in). Within the double stainless-steel encapsulation is the meltcast cesium-chloride slug measuring approximately 39.9 cm (length) by 4.8 cm (diameter) (15.7 x 1.9 in). The inner and outer walls are 0.345 cm thick (0.136 in) with total cap thicknesses of 1.016 cm (0.400 in). The walls of the capsule are constructed from 316L stainless steel. Early capsules, the type used in SIDSS, had wall thicknesses of 0.241 cm (0.095 in). Typical capsules contain about 2.4×10^{15} Bq (65 kCi) of ^{137}Cs.

Table A1.1

^{137}Cs Decay Chain Data

^{137}Cs	Half-life = 30.174 years
	Beta decay to ^{137}Ba, Q = 1.173 MeV, Branching Rate (B.R.) = 5.4 percent
	Beta decay to ^{137m}Ba, Q = 0.51163 MeV, B.R. = 94.6 percent
	(85.2 percent of ^{137}Cs decays result in a 0.66165 MeV photon)
^{137m}Ba	Half-life = 2.5513 minutes
	Gamma-ray decay to ^{137}Ba, E = 0.66165 MeV, B.R. = 89.9 percent
	Internal conversion to ^{137}Ba, E = 0.66165 MeV, B.R. = 10.1 percent.
^{137}Ba	Stable

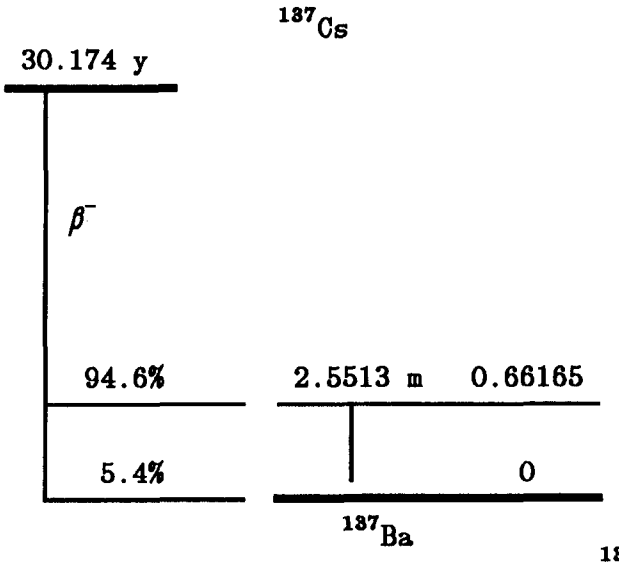

^{137}Cs

$\tau_{1/2}$: 30.174 y

β^- : 0.51163 (94.6%)
1.173 (5.4%)

γ : (see ^{137m}Ba)
0.66165 (85.0%)

^{137m}Ba

$\tau_{1/2}$: 2.5513 m

γ : 0.66165 (89.9%)

IC : 0.66165 (10.1%)

Figure A1.1. Decay Scheme for ^{137}Cs.

RADIO-ACTIVE MATERIAL	FORM	LOADING	PER CENT OF THEORETICAL DENSITY BASED ON TOTAL VOID SPACE OF CAPSULE	TEMPERATURE			
				IN AIR		IN WATER	
				CENTER LINE	SURFACE	CENTER LINE	SURFACE
CESIUM 137	MELT-CAST CESIUM CHLORIDE	65 KCi	65	450°C	200°C	327°C	58°C

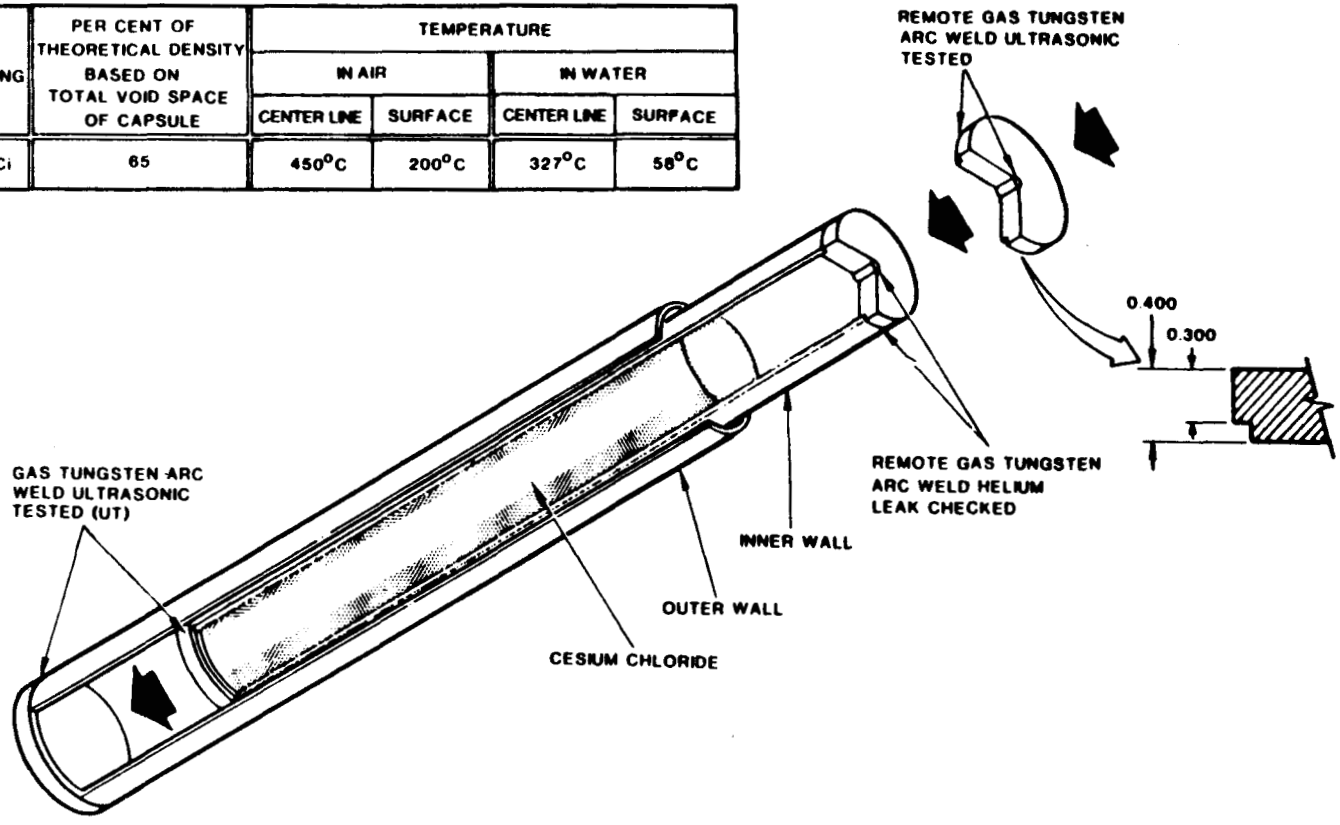

CAPSULE									
INNER					OUTER				
MATERIAL	WALL THICKNESS	OUTSIDE DIAMETER	TOTAL LENGTH	TOTAL CAP THICKNESS	MATERIAL	WALL THICKNESS	OUTSIDE DIAMETER	TOTAL LENGTH	TOTAL CAP THICKNESS
316L STAINLESS STEEL	0.136	2.250	19.725	0.400	316L STAINLESS STEEL	0.136	2.625	20.775	0.400
NOTE ALL DIMENSIONS ARE IN INCHES									APRIL 1982

Figure A1.2. WESF Cesium Chloride Source Capsule

IV. WESF SOURCE CAPSULE ENERGY DEPOSITION CALCULATIONS

Three different Monte Carlo [5,7,8,9,10] radiation transport codes, all capable of accurately modeling the WESF source capsule, have been used to determine the fraction of the emitted radiation that escapes from the WESF capsule. The MORSE-SGC,[7] CYLTRAN,[8] and MCNP [9] Monte Carlo codes were used to calculate the photon spectrum emitted from the WESF source capsule. The CYLTRAN Monte Carlo code was also used to determine the amount of electron energy that escapes from the capsule. The electrons studied include the two beta-rays, the internal conversion electrons, and any secondary electrons produced through photon interactions with the source capsule.

IV.A Photon Emission Spectrum and Photon Energy Deposition Calculations

The MORSE, CYLTRAN, and MCNP Monte Carlo codes were used to calculate the photon energy deposition in the capsule. All models were similar to the sketch of the capsule shown in Figure A1.2. Results from all three Monte Carlo transport codes agree to within a few percent. The slight discrepancies observed are due to differences in the Monte Carlo codes and possibly due to differences in the cross-sectional data sets used. For example, MORSE is a multigroup code while CYLTRAN and MCNP are continuous energy codes. This difference will affect the treatment of photon scattering and energy transfer. In addition,the CYLTRAN code is a coupled electron/photon transport code while MORSE and MCNP are not capable of charged particle transport. Therefore, the CYLTRAN results account for electron transport and some electron interactions (e.g., Bremsstrahlung radiation) that are not included in the MORSE and MCNP calculations. The cross sections used in the MORSE and CYLTRAN calculations are based on the same data set, [11] but they differ from the MCNP cross section used. This effect is thought to be small.

Regardless of which code is used, all of the results are nearly the same. Only the photon emission spectrum calculated with the MORSE code is listed in this report. The photon emission spectrum is listed as the number of photons in group g emitted from the capsule per 0.662 MeV photon born in the capsule. The energy emission and the energy deposition values are listed as fractions of the initial energy, or average energy if the radiation is in the form of a continuous spectrum, that is emitted or deposited in the capsule.

IV.A.1 MORSE-SGC Calculations

Gamma-ray microscopic cross sections for the group structure listed in Table A1.2 were generated with the GAMLEG [12] code from the BIGGS-LIGHTHILL [11] coefficient library. The ANISN format cross sections generated with GAMLEG were converted to

Table A1.2

WESF Capsule Gamma-Ray Emission Spectrum

Group (g)	Energy Bounds For Group g (Mev)	Average Energy (MeV)	Photons in Group g Per Source Photon	
1	0.660 - 0.662	0.6610	0.3416	(0.003)[a]
2	0.655 - 0.660	0.6575	0.0036	(0.034)
3	0.650 - 0.655	0.6525	0.0035	(0.032)
4	0.640 - 0.650	0.6450	0.0068	(0.024)
5	0.620 - 0.640	0.6300	0.0137	(0.017)
6	0.600 - 0.620	0.6100	0.0135	(0.017)
7	0.550 - 0.600	0.5750	0.0336	(0.010)
8	0.500 - 0.550	0.5250	0.0324	(0.011)
9	0.450 - 0.500	0.4750	0.0314	(0.011)
10	0.400 - 0.450	0.4250	0.0311	(0.010)
11	0.350 - 0.400	0.3750	0.0301	(0.010)
12	0.300 - 0.350	0.3250	0.0311	(0.011)
13	0.250 - 0.300	0.2750	0.0319	(0.010)
14	0.200 - 0.250	0.2250	0.0306	(0.010)
15	0.100 - 0.200	0.1500	0.0279	(0.010)
16	0.001 - 0.100	0.0500	0.0	(0.648)
Total			0.6628	(0.001)

[a]Fractional standard deviation.

AMPX format cross sections with the LAVA [13] code. The MORSE-SGC code was used to model the WESF capsule as shown in Figure A1.2. The WESF capsule photon emission spectrum was calculated with a modified version of the boundary crossing (BDRYX) detector package in MORSE-SGC. The energy deposited in the capsule was assumed to be the fraction of the photon energy that is not emitted from the capsule. The photon emission spectrum is listed in Table A1.2 and the energy deposition data is listed in Table A1.3.

IV.A.2 CYLTRAN WESF Capsule Calculation

The CYLTRAN continuous energy electron/photon code was used to calculate the photon emission spectrum, the photon energy deposition, and the beta-ray energy deposition for the WESF capsule. The cross sections used are based on the BIGGS-LIGHTHILL cross section file. The geometry used in the CYLTRAN calculation was identical to the geometry used in the MORSE-SGC code calculation (Figure A1.2). The energy emission data is listed in Table A1.3 and the energy deposition data is summarized in Table A1.4.

IV.A.3 MCNP Calculations

The MCNP Monte Carlo code [9] was used to calculate the photon energy emission from the WESF source capsule using wall thicknesses of both 0.136 and 0.095 in. The cross sections used are from the standard cross-sectional library (MCPLIB1) supplied with the code. Other than the wall thickness, the geometry used in the MCNP calculations was identical to the geometry used in the MORSE-SGC and CYLTRAN calculations (Figure A1.2). The photon energy emission is listed in Table A1.3.

IV.A.4 Discussion

With the exception of the calculation using a wall thickness of 0.095 in, the photon emission probabilities calculated with the MORSE, CYLTRAN, and MCNP Monte Carlo transport codes all agree to within 3 percent. The values calculated with the continuous energy codes CYLTRAN and MCNP agree to within 1 percent. The differences between the MORSE results and the CYLTRAN and MCNP results are thought to be primarily due to the multigroup approximation employed in the MORSE code.

Disregarding the calculation using a wall thickness of 0.095 in, the photon energy emission probabilities calculated with the MORSE, CYLTRAN, and MCNP Monte Carlo transport codes all agree to within 1.5 percent. The values calculated with the continuous energy codes CYLTRAN and MCNP agree to within 1 percent. Again, the differences between the MORSE results and the CYLTRAN and MCNP results are thought to be primarily due to the multigroup approximation employed in the MORSE code.

Table A1.3

WESF Capsule Radiation Emission Data

Parameter	MORSE (w.t. = 0.136 in) F[a]	MORSE FSD[b]	CYLTRAN (w.t. = 0.136 in) F[a]	CYLTRAN FSD	MCNP (w.t. = 0.136 in) F[a]	MCNP FSD	MCNP (w.t. = 0.095 in) F[a]	MCNP FSD
Photon Emission	0.663	0.001	0.680	0.01	0.674	0.002	0.716	0.002
Photon Energy Emission								
as Photons	0.540	0.002	0.547	0.01	0.544	0.002	0.601	0.002
as Electrons	n/a		0.00056	0.20	n/a		n/a	n/a
Total	0.540	0.002	0.548	0.01	0.544	0.002	0.601	0.002
Photon Energy Absorption	n/a		n/a		0.465	0.002	0.399	0.002
0.512 MeV Beta Emission	n/a		0.0	0.0	n/a		n/a	
0.512 MeV Beta Energy Emission								
as Photons	n/a		0.00013	0.34	n/a		n/a	
as Electrons	n/a		0.0	0.0	n/a		n/a	
Total	n/a		0.00013	0.34	n/a		n/a	
1.173 MeV Beta Emission	n/a		0.0	0.0	n/a		n/a	
1.173 MeV Beta Energy Emission								
as Photons	n/a		0.00252	0.05	n/a		n/a	
as Electrons	n/a		0.0	0.0	n/a		n/a	
Total	n/a		0.00252	0.05	n/a		n/a	

[a]Data listed is fraction of initial energy
[b]Fractional standard deviation

Table A1.4

WESF Capsule Energy Deposition Profile From CYLTRAN

Radiation	Deposited in CsCl F	Deposited in CsCl FSD	Deposited in SS-316L F	Deposited in SS-316L FSD	Deposited in Capsule F	Deposited in Capsule FSD
0.662 MeV Photons	0.262	0.001	0.191	0.02	0.453	0.009
0.512 MeV Beta-Rays	0.996	0.01	0.004	0.20	1.000	0.01
1.173 MeV Beta-Rays	0.987	0.01	0.011	0.13	0.998	0.01
I.C. Electrons[a]	0.996	0.01	0.004	0.20	1.000	0.01

[a]The internal conversion electron data is assumed to be the same as the 0.512 MeV beta-ray data.

IV.A.5 Electron Energy Deposition Calculations

The CYLTRAN continuous energy coupled electron/photon code was used to calculate the fraction of the electron energy that is deposited in the WESF capsule. For the two beta-ray calculations, a typical electron spectrum [3] was used. The use of this spectrum is adequate for this calculation since the results of the CYLTRAN calculations show that greater than 99.8 percent of the electron energy is deposited inside the WESF capsule. Results of the CYLTRAN calculations are listed in Tables A1.3 and A1.4. For the internal conversion electrons, it was assumed that all of the electron energy is deposited in the WESF capsule. This assumption is based on the results from the 0.512 MeV and 1.7173 MeV beta-ray calculations.

V. HEAT GENERATION IN THE WESF CAPSULE

The decay of ^{137}Cs results in the emission of photons, beta-rays, internal conversion electrons, antineutrinos,and low energy radiations. To determine the heat generation rate of a WESF capsule, three factors must be known: the strength of the WESF capsule, the radiation emitted due to the decay of ^{137}Cs and its daughter products, and the probability that the emitted radiation will deposit some or all of its energy inside the WESF capsule. In this analysis, energy deposition values will be determined relative to the decay of ^{137}Cs. Later, the heat generation rate as a function of capsule source strength will be discussed. The

types of radiation emitted from ^{137}Cs decay and the interaction probabilities have already been discussed in previous sections.

V.A. Heat Generation Per ^{137}Cs Decay

Three quantities will be computed. The first is the energy deposited in the WESF capsule per ^{137}Cs decay (E_{cap}). The second value is the energy per ^{137}Cs decay (E_{rec}) that initially escapes from the capsule but that is recoverable "near" the capsule. For example, if the capsule were located in a large storage pool, E_{rec} would be the total energy that is deposited in the capsule and in the pool. That is, the recoverable energy is all of the energy deposited as heat in the capsule, water, walls, etc. The final quantity calculated is the energy per ^{137}Cs decay emitted as antineutrinos and is therefore, nonrecoverable. The nonrecoverable energy is denoted by E_{non}.

Table A1.5 lists the ^{137}Cs decay data including branching ratios (B.R.) and decay energies. Table A1.6 lists the ^{137}Cs decay data and the Monte Carlo calculated probabilities for energy deposition in the capsule (P_{cap}). Table A1.6 also lists probabilities of recovering the decay energy (P_{rec}) and the probability of nonrecovery ($P_{non} = 1 - P_{rec}$). Finally, Table A1.7 lists the energy per ^{137}Cs decay that is deposited in the capsule (E_{cap}), the recoverable energy E_{rec}, and the nonrecoverable energy E_{non}. Table A1.7 is based on assuming that the average energy of a beta-ray is $0.3E_{max}$.[4] Some other values range from $0.28E_{max}$ to $0.41E_{max}$ [2] and from $0.29E_{max}$ to $0.30E_{max}$.[3] A 5 percent error in the value 0.3 will result in a 1.7 percent error in E_{cap}.

Table A1.5

^{137}Cs Decay Data

Radiation	Cesium B.R.	Barium B.R.	Emissions Per Decay	Decay Energy (MeV)
0.662 Photon	0.946	0.899	0.8505	0.66165
I.C. Electron	0.946	0.101	0.0955	0.66165
0.512 Beta Ray[1]	0.946	n/a	0.946	0.51163
Antineutrino[1]	0.946	n/a	0.946	0.51163
1.173 Beta Ray[2]	0.054	n/a	0.054	1.173
Antineutrino[2]	0.054	n/a	0.054	1.173

Table A1.6

^{137}Cs Decay Data and Energy Deposition Probabilities

Radiation	Emissions Per Decay	Endpoint Energy (MeV)	Average Energy (MeV)	P_{cap}	P_{rec}	P_{non}
0.662 Photon	0.8505	0.66165	0.66165	0.453	1.0	0.0
I.C. Electron	0.0955	0.66165	0.66165	1.0	1.0	0.0
0.512 Beta Ray[1]	0.946	0.51163	0.15349	1.0	1.0	0.0
Antineutrino[1]	0.946	0.51163	0.35814	0.0	0.0	1.0
1.173 Beta Ray[2]	0.054	1.173	0.35190	0.998	1.0	0.0
Antineutrino[2]	0.054	1.173	0.82110	0.0	0.0	1.0

Table A1.7

Energy Depositions Per ^{137}Cs Decay; 0.095-in Wall Thickness

Radiation	E_{cap} (MeV/Decay)	E_{rec} (MeV/Decay)	E_{non} (MeV/Decay)	E_{total} (MeV/Decay)
0.662 Photon	0.22453[a]	0.56273	0.0	0.56273
I.C. Electron	0.06319	0.06319	0.0	0.06319
0.512 Beta Ray[1]	0.14520	0.14520	0.0	0.14520
Antineutrino[1]	0.0	0.0	0.33880	0.33880
1.173 Beta Ray[2]	0.01896	0.01900	0.0	0.01900
Antineutrino[2]	0.0	0.0	0.04434	0.04434
Total	0.45186[a]	0.79012	0.38314	1.17326

[a]These values for a wall thickness of 0.136 inches are 0.25492 and 0.48225, respectively. All other values are the same for both wall thicknesses.

V.B Heat Generation for a 65 kCi WESF Capsule

To calculate the heat generation rate in watts per kCi for a WESF source capsule, the values E_{cap}, E_{rec}, and E_{non} have to be multiplied by the source strength in Bq (3.7×10^{10} Bq/kCi) and by the conversion factor 1.6022×10^{-13} J/MeV. Therefore, if S is the source strength in kCi, then the energy deposition rate in the WESF capsule (H_{cap}), measured in watts, is given by

$$H_{cap} = 2.859 \times S \ . \tag{9}$$

The recoverable energy deposition rate H_{rec}, measured in watts, is given by

$$H_{rec} = 4.684 \times S \ , \tag{10}$$

and the nonrecoverable energy deposition rate H_{non}, measured in watts, is given by

$$H \quad = 2.271 \times S \ . \tag{11}$$

For a nominal WESF source capsule of 65 kCi, the heat generation rate in the capsule with a wall thickness of 0.136 in is 185.8 watts while the total recoverable energy deposition rate is 304.5 watts. For a wall thickness of 0.095 in, the generation rate is 174.1 watts while the total recoverable energy remains at 304.5.

VI. SUMMARY

Of the total decay energy released from ^{137}Cs beta-minus decay, about 33 percent is emitted in the form of antineutrinos and is therefore nonrecoverable. About 41 percent of the decay energy is deposited directly in the WESF CsCL capsule and the remaining 26 percent escapes from the capsule mostly as photon radiation. This radiation is easily absorbed within a few feet of the capsules when they are located in large storage pools.

For nominal WESF capsules with an activity of 2.4×10^{15} Bq (65 kCi) and a wall thickness of 0.136 in, heat is generated in the capsule at the approximate rate of 185.8 watts, with an additional 118.7 watts emitted as electromagnetic radiation (photons). When the capsules are stored in a pool, they generate about 304.5 watts of heat in the pool.

REFERENCES

1. J. J. Duderstadt and L. J. Hamilton, Nuclear Reactor Analysis, (New York, NY: Wiley, 1976).

2. R. D. Evans, The Atomic Nucleus, (New York, NY: McGraw-Hill, 1955).

3. I. Kaplan, Nuclear Physics, (Reading, MA: Addison-Wesley, 1964).

4. J. R. Lamarsh, Introduction to Nuclear Engineering, (Reading, MA: Addison-Wesley, 1975).

5. N. M. Schaeffer, Reactor Shielding for Nuclear Engineers, TID-25951, (Springfield, VA: National Technical Information Service, May 1973).

6. C. M. Lederer and V. S. Shirley et al., Table of Isotopes, (New York, NY: Wiley, 1978).

7. S. A. Dupree and R. E. Lighthill, Sandia National Laboratories, CDC7600 Version of MORSE-SGC, Sandia National Laboratories, Albuquerque, NM, SAND80-1337, February 1982.

8. J. H. Halbleib, Sr. and W. H. Vandevender, CYLTRAN; A Cylindrical-Geometry Multimaterial Electron/Photon Monte Carlo Transport Code, Sandia National Laboratories, Albuquerque, NM, SAND74-0030, March 1975.

9. MCNP - A General Monte Carlo Code for Neutron and Photon Transport, Los Alamos National Laboratory, Los Alamos, NM, April 1983.

10. J. Spanier and E. M. Gelbard, Monte Carlo Principles and Neutron Transport Problems, (Reading, MA: Addison-Wesley, 1969).

11. F. Biggs and R. Lighthill, Analytical Approximations for X-Ray Cross Sections, Sandia National Laboratories, Albuquerque, NM, SC-RR-66-452, 1966.

12. J. H. Renken and K. G. Adams, An Improved Capability for Solution of Photon Transport Problems by the Method of Discrete Ordinates, Sandia National Laboratories, Albuquerque, NM, SC-RR-69-739, 1966.

13. S. K. Fraley, A User's Guide for LAVA As Issued With MORSE--SGC, Oak Ridge National Laboratory, Oak Ridge, TN: ORNL/CSD-11, June 1976.

SPECIFICATION FOR SEAMLESS 316-L AUSTENITIC-STAINLESS STEEL TUBING FOR CESIUM CHLORIDE ENCAPSULATION

1.0 SCOPE

This specification defines the requirements for seamless 316-L austenitic stainless steel tubing for radioactive cesium chloride encapsulation.

2.0 APPLICABLE DOCUMENTS

The following specifications of the issue in effect on the date of invitation for bids, shall form a part of this specification to the extent specified herein:

2.1 Specifications

American Society for Testing and Materials

A-262-64T	Recommended Practice for Detecting Susceptibility to Intergranular Attack in Austenitic Stainless Steel.
A-450-66	Specifications for General Requirements for Carbon, Ferritic Alloy and Austenitic Alloy Steel Tubes.
E-112-63	Standard Methods for Estimating the Average Grain Size of Metals.

Hanford Standard

HWS-8070-S	Standard Specification for Ultrasonic Testing of Seamless and Welded Tubing.

3.0 GENERAL

The term "lot" as used in this specification shall consist of all tubes of the same size and wall thickness which are produced from the same heat of steel and subjected to the same finishing treatment in a continuous furnace, but not to exceed 500 feet. In addition, when final heat treatment is in a batch type furnace, the "lot" shall include only those tubes which are heat treated in the same furnace charge.

4.0 REQUIREMENTS

4.1 Material

The steel shall be made by the electric furnace process.

4.1.1 Chemical Composition

The chemical composition of the steel shall be as follows:

Alloy Composition (Weight Percent)

Carbon	0.035 max.
Manganese	2.00 max.
Phosphorus	0.030 max.
Sulfur	0.030 max.
Silicon	0.75 max.
Nickel	10.0 to 15.0
Chromium	16.0 to 18.0
Molybdenum	2.0 to 3.0
Iron	Balance

4.1.2 Grain Size

The grain size of material from any "lot" after final anneal, as determined by ASTM E-112-63 Plate II, shall be five or finer.

4.1.3 Corrosion Resistance

Finished tubing shall be tested for susceptibility to intergranular attack in accordance with ASTM A262-64T, Practice B. Coupons shall be taken from each lot and shall receive a sensitizing heat treatment at 1,250 °F for 20 minutes prior to corrosion testing. Corrosion rates shall not exceed 0.004 inch per month for the 120-hour test. Only one reheat and retest of the material which fails to meet the corrosion test is permitted. Failure of retest coupons shall be a cause for rejection of the entire lot.

4.2 Heat Treatment

The tubing shall be furnished in the fully solution annealed condition.

4.3 Cleanliness of Tubing

Finished tubing shall be free from grease, oil, residual lubricants, cleaning agents, and other extraneous materials.

4.4 Mechanical Properties

The mechanical properties shall be as follows:

Annealed Tensile Property Requirements

Temperature	Minimum Tensile Strength, psi	Minimum Yield Strength 0.2% Offset, psi	Minimum Elongation in 2 in., %
Room	75,000	30,000	35
1000 °F	50,000	15,000	30

4.5 Ductility and Soundness

A section of tube taken from each lot of finished tubing shall be subjected to the following test: Finished tubing in the annealed temper shall meet the ductility and soundness requirements of the flattening test prescribed in ASTM A-450-66, Paragraph 4. Failures shall be cause for rejection of the entire lot.

4.6 Flaring

A section of tube taken from each lot of finished tubing shall be subjected to the following test: Finished tubing in the annealed temper shall show no cracking when expanded with a flaring tool as prescribed in ASTM A-450-66, Paragraph 6. Failures shall be cause for rejection of the entire lot.

4.7 Hydrostatic Test

Each finished tube shall be subjected to the following hydrostatic test: Tubing shall be tested at the mill as prescribed in ASTM A-450-66 to pressures corresponding to fiber stresses equal to 16,000 psi. Tubing shall be tested prior to dimensional and nondestructive testing, but after all thermal treatment, straightening operations, etc. Tubing exhibiting bulges, leaks, cracks, or other defects shall be rejected.

4.8 Surface Condition

The finished tubing shall be pickled free of all oxide or scale, and have smooth ends free from burrs. They shall be free from injurious defects and shall have a workmanlike finish. Minor defects may be removed by grinding, provided the wall thicknesses are not decreased to less than that permitted in section 4.10.2 of this specification.

4.9 Nondestructive Testing

Each finished tube shall be examined by the manufacturer using ultrasonic testing techniques in accordance with Hanford Standard HWS-8070-S. The ultrasonic equipment shall be calibrated by use of a qualification tube (reference standard) containing artificial internal and external, transverse and longitudinal notches of the following dimensions:

TRANSVERSE

Tubing O.D. In.	Depth, In.	Width, In.	Length, In.
2-1/4	0.006	0.005	0.250
2-5/8	0.006	0.005	0.250

LONGITUDINAL

Tubing O.D. In.	Depth, In.	Width, In.	Length, In.
2-1/4	0.006	0.005	0.500
2-5/8	0.006	0.005	0.500

The notches in the reference standard shall be machined by the buyer using tubing furnished by the seller from the production run. The buyer will deliver the reference standard to the seller for use in qualification testing. In addition, a test standard shall be furnished by the seller for each lot prepared from tubing from that lot. If all tubes of the same size and wall thickness are produced from the same heat of steel and subjected to the same finishing treatment in a continuous furnace, a test standard will not be required for each lot based on 500 feet as discussed in section 3.0 of this specification. The reference standard can be used as the test standard where this condition exists. The dimensions of the notches to be placed in the test standard shall be the

same as those listed above for the reference standard. The reference and the test standards shall become the property of, and be shipped to the buyer, at seller's expense, upon completion of the order. Permanent test records on each of the tubes are required. Tubing containing imperfections exceeding the above limits or those containing limitations shall be rejected.

4.10 Dimensions and Tolerances

4.10.1 Sizes

The nominal finished tubing sizes shall be:

a. 2-1/4 inches outside diameter by 0.095 inches wall thickness. The tubing shall be cut to minimum lengths of 19.375 inches after ultrasonic testing.

b. 2-5/8 inches outside diameter by 0.109 inches wall thickness. The tubing shall be cut to minimum lengths of 20.425 inches after ultrasonic testing.

4.10.2 Dimensional Tolerances

Variations in diameter and wall thickness shall be limited to:

a. 2-1/4 inches nominal outside diameter tubing.

2.255 inches/2.399 inches outside diameter by 0.104/0.086 inches wall thickness.

b. 2-5/8 inches nominal outside diameter tubing.

2.415 inches/2.399 inches inside diameter by 0.118 inches/0.100 inches wall thickness.

4.10.3 Eccentricity

Eccentricity shall be defined and measured as the difference between the maximum and minimum wall thickness at any cross-section. The maximum acceptable eccentricity shall be ±10 percent of nominal wall thickness.

4.10.4 Straightness

The tubing shall be free of bends and the bow shall not exceed 0.010 inch per lineal foot.

4.11 Manufacture

4.11.1 Process

Tubes shall be made by the seamless process and shall be cold drawn or tube reduced to finished size.

5.0 PREPARATION FOR DELIVERY

5.1 Marking

Each tube shall be marked with (1) manufacturer's identification, (2) alloy type, (3) this specification number, (4) heat number, and (5) lot number. The characters shall be not less than 0.250 inch in height, shall be applied using a suitable marking fluid, and shall be capable of being removed in hot alkaline cleaning solution without rubbing. The markings and cleaning solution shall have no deleterious effect on the material or its performance. The characters shall be sufficiently stable to withstand normal handling.

5.2 Packaging

Tubes shall be individually protected and packaged in rigid containers to insure delivery of straight, undamaged material. Each box shall be legibly and conspicuously marked with the following information:

Purchase Order Number
Name of Manufacturer
Alloy Type
Size
Heat and Lot
Number of tubes in the lot and number in the box

6.0 SUMMARY OF INSPECTION DATA AND MATERIAL TO BE FURNISHED THE BUYER

6.1 Certification

Two certified copies of check analysis indicating compliance with section 4.1.1 of this specification shall be furnished by buyer.

Two certified copies of test values indicating compliance with sections 4.1.2, 4.1.3, 4.4, 4.5, 4.6, 4.7, and 4.9 of this specification shall be furnished the buyer.

6.2 Test Coupon

For each lot of material, the buyer shall be furnished a coupon duplicating that used by the producer for determining compliance with section 4.1.3 of this specification.

DISTRIBUTION:

Department of Energy
Office of Defense Waste &
Transportation
Washington, DC 20545
Attn: J. J. Jicha, Jr.,
DP-132

Department of Energy (2)
Office of Remedial Action &
Waste Technology
Washington, DC 20545
Attn: J. A. Coleman, NE-24
R. B. Chitwood, NE-24

Department of Energy
Office of Security Evaluations
Washington, DC 20545
Attn: C. J. Mauck, DP-4.1

U.S. Nuclear Regulatory
Commission (2)
Division of Fuel Cycle
Washington, DC 20555
Attn: B. Carico
V. Miller

U.S. Nuclear Regulatory
Commission-Region III
799 Roosevelt Road
Glen Elly, IL 60137
Attn: B. Exilson

Department of Energy (3)
Albuquerque Operations Office
P.O. Box 5400
Albuquerque, NM 87185
Attn: C. Quinn (1)
R. Holton (2)

Department of Energy
Oak Ridge Operations Office
Oak Ridge, TN 37830
Attn: S. Wolf

Department of Energy (4)
Richland Operations Office
Richland, WA 99352
Attn: E. A. Bracken
C. R. DeLannoy
J. R. Hunter
G. W. Rosenwald

Oak Ridge National Laboratory
(2)
P.O. Box X
Oak Ridge, TN 37830
Attn: C. Ottinger
J. Setaro

A. Chin
Radiation Sterilizers, Inc.
3000 Sand Hill Road, 2-190
Menlo Park, CA 94025

B. Fairand
Radiation Sterilizers, Inc.
Westerville, OH

G. Pageau
OITECH
11080 Irma Drive
North Glen, CO 80233

E. E. Sobottka (2)
Iowa State University
Environmental Health & Safety
215 Nuclear Engineering Lab
Ames, IA 50011

R. Brown
Department of Agriculture &
Consumer Services
Division of Plant Industry
1911 S.W. 34th Street
P.O. Box 1269
Gainsville, FL 32602

CH_2M Hill (3)
6121 Indian School Road N.E.
Albuquerque, New Mexico 87110
Attn: J. Sivinski
D. Sloan
N. Ferrell

Westinghouse Hanford Company
(4)
P.O. Box 1970
Richland, WA 99352
Attn: K. A. Gasper
M. W. Gibson
I. E. Reep
M. W. Stevenson

Pacific Northwest Laboratory
(20)
P.O. Box 999
Richland WA 99352
Attn: G. H. Bryan
D. E. Eakin
R. F. Hazelton
J. H. Jarrett
H. E. Kjarmo
J. L. McElroy
A. M. Platt
G. L. Tingey (12)
E. J. Wheelwright

SANDIA DISTRIBUTION:

3141	S. A. Landenberger (5)
3151	W. L. Garner (3)
3154	C. H. Dalin (8) for DOE/OSTI
5248	B. T. Kenna
6323	J. D. Pierce
6400	D. J. McCloskey
6450	T. R. Schmidt
6454	G. L. Cano
6454	D. J. Sasmor (5)
8524	P. W. Dean